Journal of Sound and Vibration (1998) **213**(3), 483–510

WAVE REFLECTION AND TRANSMISSION IN AN AXIALLY STRAINED, ROTATING TIMOSHENKO SHAFT

C. A. TAN AND B. KANG

Department of Mechanical Engineering, Wayne State University, Detroit, MI 48202, *U.S.A.*

(*Received* 19 *May* 1997, *and in final form* 8 *January* 1998)

In this paper, the wave reflection and transmission characteristics of an axially strained, rotating Timoshenko shaft under general support and boundary conditions, and with geometric discontinuities are examined. The static axial deformation due to an axial force is also included in the model. The reflection and transmission matrices for incident waves upon these point supports and discontinuities are derived. These matrices are combined, with the aid of the transfer matrix method, to provide a concise and systematic approach for the free vibration analysis of multi-span rotating shafts with general boundary conditions. Results on the wave reflection and transmission coefficients are presented for both the Timoshenko and the simple Euler–Bernoulli models to investigate the effects of the axial strain, shaft rotation speed, shear and rotary inertia.

1. INTRODUCTION

The vibrations of elastic structures such as strings, beams, and plates can be described in terms of waves propagating and attenuating in waveguides. Although the subject of wave motions has been considered much more extensively in the field of acoustics in fluids and solids than mechanical vibrations of elastic structures, wave analysis techniques have been employed to reveal important, physical characteristics associated with vibrations of structures. One advantage of the wave technique is its compact and systematic approach to analyse complex structures such as trusses, aircraft panels with periodic supports, and beams on multiple supports [1]. Previous works based on wave propagation techniques have been well documented in several books [2–4]. Recently, Mead [5] applied the phase-closure principle to determine the natural frequencies of Euler–Bernoulli beam models. A systematic approach including both the propagating and near-field waves was employed to study the free vibrations of Euler–Bernoulli beams [6].

High speed rotating shafts are commonly employed in precision manufacturing and power transmission. Despite the usefulness of the wave propagation method in structural vibrations, applications of this technique to study the dynamics and vibrations of a flexible shaft rotating about its longitudinal axis have seldom been considered. The purpose of this paper is to examine the wave reflection and transmission [6] in an axially strained, rotating Timoshenko shaft under various support and boundary conditions. The effect of the axial load is included by considering the axial static deformations in the equations of motion. This paper is a sequel to another paper in which the authors discuss the basic wave motions in the infinitely long shaft model [7].

0022–460X/98/230483 + 28 $25.00/0/sv981517

Although there have been numerous studies on the dynamics and vibration of rotating shafts, none has examined the effects of axial strains (which cannot be neglected in many applications) on the vibration characteristics of a Timoshenko shaft under multiple supports. The modal analysis technique has been applied to study the vibration of a rotating Timoshenko shaft with general boundary conditions [8, 9], and subject to a moving load [10]. Recently, the distributed transfer function method was applied to a rotating shaft system with multiple, geometric discontinuities [11]. The wave propagation in a rotating Timoshenko shaft was considered in reference [12]. Other major works on the dynamics of rotating shafts have been well documented in references [13–15].

This paper is organized as follows. Governing equations of motion [16] and basic wave solutions for the Timoshenko shaft are outlined in section 2. Each wave solution consists of four wave components: positive and negative, propagating and attenuating waves. In section 3, the wave reflection and transmission matrices are derived for the shaft under various point supports. The supports may include translational and rotational springs and dampers, and a rotor mass. Results are presented for both the Timoshenko and the simple Euler–Bernoulli models to assess the effects of axial strain, shaft rotation, shear and rotary inertia. The wave propagation across a shaft with geometric discontinuities such as a change in the cross-section is examined in section 4, and the wave reflection at a boundary with arbitrary support conditions is considered in section 5. With the wave reflection and transmission matrices as the main analytical tools, it is shown in section 6 how to apply the current results together with the transfer matrix method to analyse the free vibration of a rotating, multi-span Timoshenko shaft system in a systematic manner.

2. FORMULATION AND WAVE SOLUTIONS

Consider a rotating shaft subjected to axial loads and with multiple intermediate supports and arbitrary boundary conditions, as shown in Figure 1. Including the effects of rotary inertia, shear deformations, and axial deformations due to the axial loads, the uncoupled equations of motion governing the transverse displacement u and the slope ψ due to bending can be derived in the following non-dimensional form:

$$\frac{\partial^4 u}{\partial z^4} - (1+\alpha)\frac{\partial^4 u}{\partial z^2\,\partial t^2} + 2\mathrm{i}\beta\frac{\partial^3 u}{\partial z^2\,\partial t} - 2\mathrm{i}\beta\frac{\partial^3 u}{\partial t^3} + \alpha\frac{\partial^4 u}{\partial t^4} - 16\varepsilon\left(1+\varepsilon-\frac{\varepsilon}{\alpha}\right)\frac{\partial^2 u}{\partial z^2}$$

$$+ 16\alpha(1+\varepsilon)\left(1+\varepsilon-\frac{\varepsilon}{\alpha}\right)\frac{\partial^2 u}{\partial t^2} = 0, \quad (1a)$$

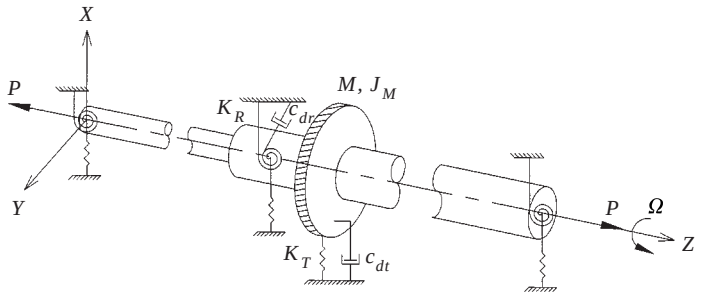

Figure 1. A rotating Timoshenko shaft model subject to axial loads and with general boundary conditions.

$$\frac{\partial^4\psi}{\partial z^4} - (1+\alpha)\frac{\partial^4\psi}{\partial z^2\,\partial t^2} + 2\mathrm{i}\beta\frac{\partial^3\psi}{\partial z^2\,\partial t} - 2\mathrm{i}\beta\frac{\partial^3\psi}{\partial t^3} + \alpha\frac{\partial^4\psi}{\partial t^4} - 16\varepsilon\left(1+\varepsilon-\frac{\varepsilon}{\alpha}\right)\frac{\partial^2\psi}{\partial z^2}$$

$$+ 16\alpha(1+\varepsilon)\left(1+\varepsilon-\frac{\varepsilon}{\alpha}\right)\frac{\partial^2\psi}{\partial t^2} = 0, \tag{1b}$$

where

$$u = \frac{U}{a_0}, \qquad z = \frac{Z}{a_0}, \qquad t = \frac{T}{T_0}, \qquad T_0 = \sqrt{\frac{\rho a_0^2}{KG}}, \tag{1c}$$

$$\alpha = \frac{KG}{E}, \qquad \beta = \frac{\rho a_0^2}{ET_0}\,\Omega = \frac{\rho a_0\, c_s}{E}\,\Omega, \qquad \varepsilon = \frac{P}{EA_s}. \tag{1d}$$

Note that u and ψ are the measurements in the complex plane, that is $u = u_x + \mathrm{i}u_y$ and $\psi = \psi_x + \mathrm{i}\psi_y$, $i = \sqrt{-1}$, E denotes the Young's modulus, ρ the mass density, A_s the area of the cross-section, a_0 the diameter of shaft, K the Timoshenko shear coefficient, G the shear modulus and Ω the constant angular velocity of the shaft. Details of deriving these equations of motion are found in reference [16].

Assuming and substituting the following wave solutions into equations (1a) and (1b)

$$u(z,t) = C_u\,\mathrm{e}^{\mathrm{i}(\bar{\gamma}z + \bar{\omega}t)}, \qquad \psi(z,t) = C_\psi\,\mathrm{e}^{\mathrm{i}(\bar{\gamma}z + \bar{\omega}t)}, \tag{2a, b}$$

and defining the non-dimensionalized wavenumber $\bar{\gamma}$ and frequency $\bar{\omega}$ gives the frequency equation (3a); see reference [7],

$$\bar{\gamma} = \gamma a_0, \qquad \bar{\omega} = \frac{\omega a_0}{c_s} \qquad (c_s = \sqrt{KG/\rho} \text{ is known as the shear velocity}). \tag{2c, d}$$

$$\bar{\gamma}^4 - A\bar{\gamma}^2 + B = 0, \tag{3a}$$

where

$$A = (1+\alpha)\bar{\omega}^2 - 2\beta\bar{\omega} - 16\varepsilon\left(1+\varepsilon-\frac{\varepsilon}{\alpha}\right), \tag{3b}$$

$$B = \bar{\omega}^2\left[\alpha\bar{\omega}^2 - 2\beta\bar{\omega} - 16\alpha(1+\varepsilon)\left(1+\varepsilon-\frac{\varepsilon}{\alpha}\right)\right]. \tag{3c}$$

The four roots of equation (3a) are

$$\bar{\gamma} = \pm\frac{1}{\sqrt{2}}(A \pm \sqrt{A^2 - 4B})^{1/2}. \tag{4}$$

In general, $\bar{\gamma}$ is complex. Let $\bar{\omega}$ be real. It can be shown that, with $\alpha > 0$ and ε the axial strain of the elastic solid, the discriminant $A^2 - 4B$ is positive semi-definite for most engineering applications. Hence, it is possible to classify the wave solutions into four distinct cases. Note that one may study the wave propagation by considering only a single general form of the wave solution. However, the classification procedure identifies the coupled modes of vibration of the Timoshenko shaft model and provides a better understanding on how each wave solution governs the wave motions [7]. Based on the algebraic relationships between A and B, the four valid wave solutions are obtained as follows.

Case I ($A > 0$ and $B > 0$):

$$u(z, t) = (C_{u1}^{+}\, e^{-i\bar{\gamma}_1 z} + C_{u1}^{-}\, e^{i\bar{\gamma}_1 z} + C_{u2}^{+}\, e^{-i\bar{\gamma}_2 z} + C_{u2}^{-}\, e^{i\bar{\gamma}_2 z})\, e^{i\tilde{\omega}t}, \tag{5a}$$

$$\psi(z, t) = (C_{\psi 1}^{+}\, e^{-i\bar{\gamma}_1 z} + C_{\psi 1}^{-}\, e^{i\bar{\gamma}_1 z} + C_{\psi 2}^{+}\, e^{-i\bar{\gamma}_2 z} + C_{\psi 2}^{-}\, e^{i\bar{\gamma}_2 z})\, e^{i\tilde{\omega}t}; \tag{5b}$$

Case II ($A > 0$ and $B < 0$):

$$u(z, t) = (C_{u1}^{+}\, e^{-i\bar{\Gamma}_1 z} + C_{u1}^{-}\, e^{i\bar{\Gamma}_1 z} + C_{u2}^{+}\, e^{-\bar{\Gamma}_2 z} + C_{u2}^{-}\, e^{\bar{\Gamma}_2 z})\, e^{i\tilde{\omega}t}, \tag{6a}$$

$$\psi(z, t) = (C_{\psi 1}^{+}\, e^{-i\bar{\Gamma}_1 z} + C_{\psi 1}^{-}\, e^{i\bar{\Gamma}_1 z} + C_{\psi 2}^{+}\, e^{-\bar{\Gamma}_2 z} + C_{\psi 2}^{-}\, e^{\bar{\Gamma}_2 z})\, e^{i\tilde{\omega}t}; \tag{6b}$$

Case III ($A < 0$ and $B > 0$):

$$u(z, t) = (C_{u1}^{+}\, e^{-\bar{\gamma}_1 z} + C_{u1}^{-}\, e^{\bar{\gamma}_1 z} + C_{u2}^{+}\, e^{-\bar{\gamma}_2 z} + C_{u2}^{-}\, e^{\bar{\gamma}_2 z})\, e^{i\tilde{\omega}t}, \tag{7a}$$

$$\psi(z, t) = (C_{\psi 1}^{+}\, e^{-\bar{\gamma}_1 z} + C_{\psi 1}^{-}\, e^{\bar{\gamma}_1 z} + C_{\psi 2}^{+}\, e^{-\bar{\gamma}_2 z} + C_{\psi 2}^{-}\, e^{\bar{\gamma}_2 z})\, e^{i\tilde{\omega}t}; \tag{7b}$$

Case IV ($A < 0$ and $B < 0$):

$$u(z, t) = (C_{u1}^{+}\, e^{-\bar{\Gamma}_1 z} + C_{u1}^{-}\, e^{\bar{\Gamma}_1 z} + C_{u2}^{+}\, e^{-i\bar{\Gamma}_2 z} + C_{u2}^{-}\, e^{i\bar{\Gamma}_2 z})\, e^{i\tilde{\omega}t}, \tag{8a}$$

$$\psi(z, t) = (C_{\psi 1}^{+}\, e^{-\bar{\Gamma}_1 z} + C_{\psi 1}^{-}\, e^{\bar{\Gamma}_1 z} + C_{\psi 2}^{+}\, e^{-i\bar{\Gamma}_2 z} + C_{\psi 2}^{-}\, e^{i\bar{\Gamma}_2 z})\, e^{i\tilde{\omega}t}; \tag{8b}$$

where

$$\bar{\gamma}_1 = \frac{1}{\sqrt{2}}(|A| + \sqrt{A^2 - 4|B|})^{1/2}, \qquad \bar{\gamma}_2 = \frac{1}{\sqrt{2}}(|A| - \sqrt{A^2 - 4|B|})^{1/2}, \tag{9a, b}$$

$$\bar{\Gamma}_1 = \frac{1}{\sqrt{2}}(\sqrt{A^2 + 4|B|} + |A|)^{1/2}, \qquad \bar{\Gamma}_2 = \frac{1}{\sqrt{2}}(\sqrt{A^2 + 4|B|} - |A|)^{1/2}, \tag{9c, d}$$

and the coefficients C^{+} and C^{+} denote positive- and negative-travelling waves from the origin of disturbance, respectively. Important remarks on the basic wave propagation characteristics are summarized from reference [7]. First, the wave solution of *Case III* does not exist in the real frequency space since this type of solution represents a situation in which none of the wave components can propagate along the waveguide. Therefore the study of *Case III* is excluded in the present paper. Second, the vibrating motion of the shaft model in *Case I* is predominately simple and pure shear modes [17] which are unique for the Timoshenko shaft model, while in *Cases II* and *IV* the Euler–Bernoulli mode and the simple shear mode dominate at low and high wavenumber, respectively. Third, when the shaft rotates at a very high speed and/or the shaft is axially strained by tensile loads, the wave solution of *Case IV* governs the vibrating motion of the shaft model in the low frequency range.

For comparison, the parameters A and B in the simple Euler–Bernoulli beam model are

$$A = -2\beta\tilde{\omega} - 16\varepsilon, \qquad B = -16\tilde{\omega}^2, \tag{10a, b}$$

where the non-dimensionalized frequency $\tilde{\omega}$ is defined as

$$\tilde{\omega} = \frac{\omega a_0}{c_0} \quad (c_0 = \sqrt{E/\rho} \text{ is known as the } \textit{bar velocity}). \tag{10c}$$

Note that, because B is negative, wave solutions of *Cases I* and *III* do not exist.

In general the displacement and the rotation of an infinitesimal shaft element consist of four wave components as shown by equations (5a–8b). Once the displacement and the bending slope are known, the moment M and shear force V at a cross-section can be determined from

$$M = EI\frac{\partial \psi}{\partial z}, \qquad V = KAG\left(\frac{\partial u}{\partial z} + \mathrm{i}\psi\right). \tag{11, 12}$$

Moreover, the kinematic relationship between the transverse displacement and the slope due to bending is

$$\frac{\partial^2 u}{\partial t^2} = \frac{\partial^2 u}{\partial z^2} + \mathrm{i}\varepsilon'\frac{\partial \psi}{\partial z}, \tag{13a}$$

where ε' denotes the effects of the axial force and is defined as

$$\varepsilon' = 1 + \varepsilon - \varepsilon/\alpha. \tag{13b}$$

3. WAVE REFLECTION AND TRANSMISSION AT SUPPORTS

When a wave is incident upon a discontinuity, it is transmitted and reflected at different rates depending on the properties of the discontinuity. Consider a rotating Timoshenko shaft model supported at $z = 0$; see Figure 2. The support simulates a bearing modelled by linear, translational and rotational springs, dampers, and a rotor mass which typically represents a gear transmitting a torque. Based on equations (5a–8b), group the four wave components into 2×1 vectors of positive-travelling waves $\mathbf{C}^+$ and negative-travelling waves $\mathbf{C}^-$, i.e.,

$$\mathbf{C}^+ = \begin{Bmatrix} C_1^+ \\ C_2^+ \end{Bmatrix}, \qquad \mathbf{C}^- = \begin{Bmatrix} C_1^- \\ C_2^- \end{Bmatrix}. \tag{14a, b}$$

Recall that, depending on the system parameters, the rotating Timoshenko shaft model has four (practically three) different wave solutions in the entire frequency region as described in equations (5a–8b). Thus, C_1 and C_2 in the above expression do not always

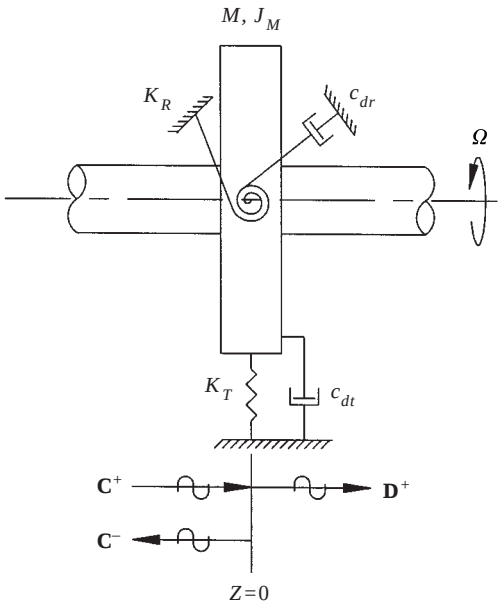

Figure 2. Wave motion at a general support (the disk may be considered as a gear transmitting a torque): $u(z) = C_{u1}^+ \mathrm{e}^{-\mathrm{i}\Gamma_1 z} + C_{u1}^- \mathrm{e}^{-\mathrm{i}\Gamma_1 z} + C_{u2}^+ \mathrm{e}^{-\mathrm{i}\Gamma_2 z} + C_{u2}^- \mathrm{e}^{\mathrm{i}\Gamma_2 z}$ (for *Case II*), $u^+(z) = D_{u1}^+ \mathrm{e}^{-\mathrm{i}\Gamma_1 z} + D_{u2}^+ \mathrm{e}^{-\mathrm{i}\Gamma_2 z}$.

correspond to propagating and attenuating wave components, respectively. When a set of positive-travelling waves $\mathbf{C}^+$ is incident upon the support, it gives rise to a set of reflected waves $\mathbf{C}^-$ and transmitted waves $\mathbf{D}^+$. These waves are related by

$$\mathbf{C}^- = \mathbf{r}\mathbf{C}^+, \qquad \mathbf{D}^+ = \mathbf{t}\mathbf{C}^+, \tag{15, 16}$$

where $\mathbf{r}$ and $\mathbf{t}$ are the 2×2 reflection and transmission matrices respectively and are expressed as

$$\mathbf{r} = \begin{bmatrix} r_{11} & r_{12} \\ r_{21} & r_{22} \end{bmatrix}, \qquad \mathbf{t} = \begin{bmatrix} t_{11} & t_{12} \\ t_{21} & t_{22} \end{bmatrix}. \tag{17, 18}$$

From equations (5a–8b), suppressing the $e^{i\omega t}$ term and excluding *Case III*, the displacements u^- and u^+ and the bending slopes ψ^- and ψ^+ at the left and right of $z = 0$, respectively, can be expressed in terms of the wave amplitudes of the displacement. For convenience, the over-bar ($\bar{\ }$) on the wavenumbers is dropped hereafter.

Case I ($A > 0$ and $B > 0$):

$$u^-(z) = C_{u1}^+ e^{-i\gamma_1 z} + C_{u1}^- e^{i\gamma_1 z} + C_{u2}^+ e^{-i\gamma_2 z} + C_{u2}^- e^{i\gamma_2 z}, \tag{19a}$$

$$\psi^-(z) = \eta_1 C_{u1}^+ e^{-i\gamma_1 z} - \eta_1 C_{u1}^- e^{i\gamma_1 z} + \eta_2 C_{u2}^+ e^{-i\gamma_2 z} - \eta_2 C_{u2}^- e^{i\gamma_2 z}, \tag{19b}$$

$$u^+(z) = D_{u1}^+ e^{-i\gamma_1 z} + D_{u2}^+ e^{-i\gamma_2 z}, \qquad \psi^+(z) = \eta_1 D_{u1}^+ e^{-i\gamma_1 z} + \eta_2 D_{u2}^+ e^{-i\gamma_2 z}, \tag{19c, d}$$

where

$$\eta_1 = \frac{\gamma_1^2 - \omega^2}{\gamma_1 \varepsilon'}, \qquad \eta_2 = \frac{\gamma_2^2 - \omega^2}{\gamma_2 \varepsilon'}. \tag{20a, b}$$

Case II ($A > 0$ and $B < 0$):

$$u^-(z) = C_{u1}^+ e^{-i\Gamma_1 z} + C_{u1}^- e^{i\Gamma_1 z} + C_{u2}^+ e^{-\Gamma_2 z} + C_{u2}^- e^{\Gamma_2 z}, \tag{21a}$$

$$\psi^-(z) = \eta_1 C_{u1}^+ e^{-i\Gamma_1 z} - \eta_1 C_{u1}^- e^{i\Gamma_1 z} + \eta_2 C_{u2}^+ e^{-\Gamma_2 z} - \eta_2 C_{u2}^- e^{\Gamma_2 z}, \tag{21b}$$

$$u^+(z) = D_{u1}^+ e^{-i\Gamma_1 z} + D_{u2}^+ e^{-\Gamma_2 z}, \qquad \psi^+(z) = \eta_1 D_{u1}^+ e^{-i\Gamma_1 z} + \eta_2 D_{u2}^+ e^{-\Gamma_2 z}, \tag{21c, d}$$

where

$$\eta_1 = \frac{\Gamma_1^2 - \omega^2}{\Gamma_1 \varepsilon'}, \qquad \eta_2 = \frac{\Gamma_2^2 + \omega^2}{i\Gamma_2 \varepsilon'}. \tag{22a, b}$$

Case IV ($A < 0$ and $B < 0$):

$$u^-(z) = C_{u1}^+ e^{-\Gamma_1 z} + C_{u1}^- e^{\Gamma_1 z} + C_{u2}^+ e^{-i\Gamma_2 z} + C_{u2}^- e^{i\Gamma_2 z}, \tag{23a}$$

$$\psi^-(z) = \eta_1 C_{u1}^+ e^{-\Gamma_1 z} - \eta_1 C_{u1}^- e^{\Gamma_1 z} + \eta_2 C_{u2}^+ e^{-i\Gamma_2 z} - \eta_2 C_{u2}^- e^{i\Gamma_2 z}, \tag{23b}$$

$$u^+(z) = D_{u1}^+ e^{-\Gamma_1 z} + D_{u2}^+ e^{-i\Gamma_2 z}, \qquad \psi^+(z) = \eta_1 D_{u1}^+ e^{-\Gamma_1 z} + \eta_2 D_{u2}^+ e^{-i\Gamma_2 z}, \tag{23c, d}$$

where

$$\eta_1 = \frac{\Gamma_1^2 + \omega^2}{i\Gamma_1 \epsilon'}, \qquad \eta_2 = \frac{\Gamma_2^2 - \omega^2}{\Gamma_2 \epsilon'}. \tag{24a, b}$$

Introducing the non-dimensional parameters

$$k_t = \frac{K_t a_0}{KAG}, \quad k_r = \frac{K_r a_0}{EI}, \quad c_t = \frac{c_{dt} c_s}{KAG}, \quad c_r = \frac{c_{dr} c_s}{EI}, \quad m = \frac{M}{\rho A a_0} \quad \text{and} \quad J_m = \frac{J_M c_s^2}{EI}, \tag{25}$$

and by imposing the geometric continuity

$$u^-(0) = u^+(0), \qquad \psi^-(0) = \psi^+(0) \tag{26a, b}$$

and the moment and force balance conditions at the support,

$$M^- - M^+ = k_r\,\psi + c_r\,\dot{\psi} + J_m\,\ddot{\psi}, \qquad V^+ - V^- = k_t\,u + c_t\,\dot{u} + m\ddot{u}, \tag{27a, b}$$

the following set of matrix equations can be established for each *Case*.

Case I ($A > 0$ and $B > 0$):

$$\begin{bmatrix} 1 & 1 \\ \eta_1 & \eta_2 \end{bmatrix}\mathbf{C}^+ + \begin{bmatrix} 1 & 1 \\ -\eta_1 & -\eta_2 \end{bmatrix}\mathbf{r}\mathbf{C}^+ = \begin{bmatrix} 1 & 1 \\ \eta_1 & \eta_2 \end{bmatrix}\mathbf{t}\mathbf{C}^+, \tag{28a}$$

$$\begin{bmatrix} -\mathrm{i}\gamma_1\,\eta_1 & -\mathrm{i}\gamma_2\,\eta_2 \\ \mathrm{i}(\gamma_1 - \eta_1) & \mathrm{i}(\gamma_2 - \eta_2) \end{bmatrix}\mathbf{C}^+ + \begin{bmatrix} -\mathrm{i}\gamma_1\,\eta_1 & -\mathrm{i}\gamma_2\,\eta_2 \\ -\mathrm{i}(\gamma_1 - \eta_1) & -\mathrm{i}(\gamma_2 - \eta_2) \end{bmatrix}\mathbf{r}\mathbf{C}^+$$

$$= \begin{bmatrix} \eta_1\,(k_r - J_m\,\omega^2) + \mathrm{i}\eta_1\,(c_r\,\omega - \gamma_1) & \eta_2\,(k_r - J_m\,\omega^2) + \mathrm{i}\eta_2\,(c_r\,\omega - \gamma_2) \\ (k_t - m\omega^2) + \mathrm{i}(c_t\,\omega + \gamma_1 - \eta_1) & (k_t - m\omega^2) + \mathrm{i}(c_t\,\omega + \gamma_2 - \eta_2) \end{bmatrix}\mathbf{t}\mathbf{C}^+; \tag{28b}$$

Case II ($A > 0$ and $B < 0$):

$$\begin{bmatrix} 1 & 1 \\ \eta_1 & \eta_2 \end{bmatrix}\mathbf{C}^+ + \begin{bmatrix} 1 & 1 \\ -\eta_1 & -\eta_2 \end{bmatrix}\mathbf{r}\mathbf{C}^+ = \begin{bmatrix} 1 & 1 \\ \eta_1 & \eta_2 \end{bmatrix}\mathbf{t}\mathbf{C}^+, \tag{29a}$$

$$\begin{bmatrix} -\mathrm{i}\Gamma_1\,\eta_1 & -\Gamma_2\,\eta_2 \\ \mathrm{i}(\Gamma_1 - \eta_1) & \Gamma_2 - \mathrm{i}\eta_2 \end{bmatrix}\mathbf{C}^+ + \begin{bmatrix} -\mathrm{i}\Gamma_1\,\eta_1 & -\Gamma_2\,\eta_2 \\ -\mathrm{i}(\Gamma_1 - \eta_1) & -(\Gamma_2 - \mathrm{i}\eta_2) \end{bmatrix}\mathbf{r}\mathbf{C}^+$$

$$= \begin{bmatrix} \eta_1\,(k_r - J_m\,\omega^2) + \mathrm{i}\eta_1\,(c_r\,\omega - \gamma_1) & \eta_2\,(k_r - J_m\,\omega^2 - \gamma_2) + \mathrm{i}\eta_2\,c_r\,\omega \\ (k_t - m\omega^2) + \mathrm{i}(c_t\,\omega + \Gamma_1 - \eta_1) & (k_t - m\omega^2 + \Gamma_2) + \mathrm{i}(c_t\,\omega - \eta_2) \end{bmatrix}\mathbf{t}\mathbf{C}^+; \tag{29b}$$

Case IV ($A < 0$ and $B > 0$):

$$\begin{bmatrix} 1 & 1 \\ \eta_2 & \eta_1 \end{bmatrix}\mathbf{C}^+ + \begin{bmatrix} 1 & 1 \\ -\eta_2 & -\eta_1 \end{bmatrix}\mathbf{r}\mathbf{C}^+ = \begin{bmatrix} 1 & 1 \\ \eta_2 & \eta_1 \end{bmatrix}\mathbf{t}\mathbf{C}^+, \tag{30a}$$

$$\begin{bmatrix} -\mathrm{i}\Gamma_2\,\eta_2 & -\mathrm{i}\Gamma_1\,\eta_1 \\ \mathrm{i}(\Gamma_2 - \eta_2) & \Gamma_1 - \mathrm{i}\eta_1 \end{bmatrix}\mathbf{C}^+ + \begin{bmatrix} -\mathrm{i}\Gamma_2\,\eta_2 & -\mathrm{i}\Gamma_1\,\eta_1 \\ -\mathrm{i}(\Gamma_2 - \eta_2) & -(\Gamma_1 - \mathrm{i}\eta_1) \end{bmatrix}\mathbf{r}\mathbf{C}^+$$

$$= \begin{bmatrix} \eta_2\,(k_r - J_m\,\omega^2) + \mathrm{i}\eta_2\,(c_r\,\omega - \gamma_2) & \eta_1\,(k_r - J_m\,\omega^2 - \gamma_1) + \mathrm{i}\eta_1\,c_r\,\omega \\ (k_t - m\omega^2) + \mathrm{i}(c_t\,\omega + \Gamma_2 - \eta_2) & (k_t - m\omega^2 + \Gamma_1) + \mathrm{i}(c_t\,\omega - \eta_1) \end{bmatrix}\mathbf{t}\mathbf{C}^+; \tag{30b}$$

where equations (15) and (16) have been applied in all *Cases*. Note that in equation (27a), it is assumed that the rotational spring at the support is attached to the cross-section of a shaft element such that the rotational spring responds only to the slope change due to rotation of the cross-section and not the total slope change of the neutral axis of the shaft model. This assumption allows the shearing motion of the shaft element at the support.

Note also that the effect of axial loads on the shear force at the support is neglected since the contribution of axial loads to the shear force at the support or boundary is small compared to the shear force due to the flexural motion of the shaft element. Exact moment and force balance conditions at boundaries for a rotating Timoshenko shaft element subjected to axial loads can be found in reference [16].

The corresponding matrix equations for the simple Euler–Bernoulli shaft model are shown in Appendix A. Solving the set of matrix equations simultaneously for **r** and **t** gives the elements of the reflection and transmission for each *Case*. The general forms of solutions to these sets of equations for each *Case* is not presented in this paper due to space limitation. However one can obtain the solutions in either closed-form or numerically. Note that in *Cases II* and *IV*, the first columns of **r** and **t** are the reflection and transmission coefficients due to incident propagating wave components, and the second columns are due to an incident attenuating wave component which is generally termed as *near-field* since this type of wave decays exponentially with distance. When the distance between the origin of disturbance and the discontinuity is very large, these attenuating wave components can be neglected. However, as mentioned by many authors, for example Graff [2], attenuating waves play an important role in wave motion by contributing a significant amount of energy to the propagating wave components when a set of propagating and attenuating waves are incident at a discontinuity and, in particular, when the distances between the discontinuities are relatively small, as in the case of closely-spaced multi-span beams. In this paper, near-field components are included. In what follows, the effects of the point supports on the reflection and transmission of an incident wave are studied. For comparison, the results are obtained for both the Timoshenko and the simple Euler–Bernoulli models, which hereafter, for brevity, are denoted by TM and E-B, respectively. The system parameters used in the numerical results are taken from reference [10]: $a_0 = 0{\cdot}0955$ m, $\rho = 7700$ kg/m^3, $K = 0{\cdot}9$, $E = 207 \times 10^9$ N/m^2, $G = 77{\cdot}7 \times 10^9$ N/m^2.

3.1. WAVE REFLECTION AND TRANSMISSION AT RIGID SUPPORTS

Consider two cases: the simple support and the clamped support. The **r** and **t** are solved and shown as follows.

Simple support ($k_t = \infty$, $k_r = m = c_t = c_r = J_m = 0$)

Case I ($A > 0$ and $B > 0$)

$$\mathbf{r} = \frac{1}{(\gamma_2 - \gamma_1)(\gamma_1\gamma_2 + \omega^2)} \begin{bmatrix} \gamma_1(\omega^2 - \gamma_2^2) & \gamma_1(\omega^2 - \gamma_2^2) \\ \gamma_2(\gamma_1^2 - \omega^2) & \gamma_2(\gamma_1^2 - \omega^2) \end{bmatrix}, \tag{31a}$$

$$\mathbf{t} = \frac{1}{(\gamma_2 - \gamma_1)(\gamma_1\gamma_2 + \omega^2)} \begin{bmatrix} \gamma_2(\omega^2 - \gamma_1^2) & \gamma_1(\omega^2 - \gamma_2^2) \\ \gamma_2(\gamma_1^2 - \omega^2) & \gamma_1(\gamma_2^2 - \omega^2) \end{bmatrix}; \tag{31b}$$

Case II ($A > 0$ and $B < 0$):

$$\mathbf{r} = \frac{1}{(\mathrm{i}\Gamma_1 - \Gamma_2)(\Gamma_1\Gamma_2 - \mathrm{i}\omega^2)} \begin{bmatrix} \Gamma_1(\Gamma_2^2 + \omega^2) & \Gamma_1(\Gamma_2^2 + \omega^2) \\ -\mathrm{i}\Gamma_2(\Gamma_1^2 - \omega^2) & -\mathrm{i}\Gamma_2(\Gamma_1^2 - \omega^2) \end{bmatrix}, \tag{32a}$$

$$\mathbf{t} = \frac{1}{(\mathrm{i}\Gamma_1 - \Gamma_2)(\Gamma_1\Gamma_2 - \mathrm{i}\omega^2)} \begin{bmatrix} \mathrm{i}\Gamma_2(\Gamma_1^2 - \omega^2) & \Gamma_1(\Gamma_2^2 + \omega^2) \\ -\mathrm{i}\Gamma_2(\Gamma_1^2 - \omega^2) & -\Gamma_1(\Gamma_2^2 + \omega^2) \end{bmatrix}; \tag{32b}$$

Case IV ($A < 0$ and $B < 0$)

$$\mathbf{r} = \frac{1}{(\Gamma_1 - \mathrm{i}\Gamma_2)(\Gamma_1\Gamma_2 + \mathrm{i}\omega^2)}\begin{bmatrix} \Gamma_2(\Gamma_1^2 + \omega^2) & \Gamma_2(\Gamma_1^2 + \omega^2) \\ -\mathrm{i}\Gamma_1(\Gamma_2^2 - \omega^2) & -\mathrm{i}\Gamma_1(\Gamma_2^2 - \omega^2) \end{bmatrix}, \tag{33a}$$

$$\mathbf{t} = \frac{1}{(\Gamma_1 - \mathrm{i}\Gamma_2)(\Gamma_1\Gamma_2 + \mathrm{i}\omega^2)}\begin{bmatrix} \mathrm{i}\Gamma_1(\Gamma_2^2 - \omega^2) & \Gamma_2(\Gamma_1^2 + \omega^2) \\ -\mathrm{i}\Gamma_1(\Gamma_2^2 - \omega^2) & -\Gamma_2(\Gamma_1^2 + \omega^2) \end{bmatrix}. \tag{33b}$$

Clamped support ($k_t = \infty$, $k_r = \infty$, $m = c_t = c_r = J_m = 0$); in all cases $\mathbf{t} = 0$ because no wave can be transmitted through the rigid constraints.

Case I ($A > 0$ and $B > 0$):

$$\mathbf{r} = \frac{1}{(\gamma_1 - \gamma_2)(\gamma_1\gamma_2 + \omega^2)}\begin{bmatrix} (\gamma_1 + \gamma_2)(\gamma_1\gamma_2 - \omega^2) & 2\gamma_1(\gamma_2^2 - \omega^2) \\ -2\gamma_2(\gamma_1^2 - \omega^2) & -(\gamma_1 + \gamma_2)(\gamma_1\gamma_2 - \omega^2) \end{bmatrix}; \tag{34}$$

Case II ($A > 0$ and $B < 0$):

$$\mathbf{r} = \frac{1}{(\Gamma_1 + \mathrm{i}\Gamma_2)(\Gamma_1\Gamma_2 + \mathrm{i}\omega^2)}\begin{bmatrix} (\Gamma_1 - \mathrm{i}\Gamma_2)(\Gamma_1\Gamma_2 - \mathrm{i}\omega^2) & -2\mathrm{i}\Gamma_1(\Gamma_2^2 + \omega^2) \\ -2\Gamma_2(\Gamma_1^2 - \omega^2) & (\Gamma_1 - \mathrm{i}\Gamma_2)(\omega^2 - \Gamma_1\Gamma_2) \end{bmatrix}; \tag{35}$$

Case IV ($A < 0$ and $B < 0$):

$$\mathbf{r} = \frac{1}{(\Gamma_1 - \mathrm{i}\Gamma_2)(\Gamma_1\Gamma_2 + \mathrm{i}\omega^2)}\begin{bmatrix} (\Gamma_1 + \mathrm{i}\Gamma_2)(\mathrm{i}\omega^2 - \Gamma_1\Gamma_2) & -2\Gamma_2(\Gamma_1^2 + \omega^2) \\ 2\mathrm{i}\Gamma_1(\Gamma_2^2 - \omega^2) & (\Gamma_1 + \mathrm{i}\Gamma_2)(\Gamma_1\Gamma_2 - \mathrm{i}\omega^2) \end{bmatrix}. \tag{36}$$

The corresponding reflection and transmission matrices for the E-B model are listed in Appendix A.

Figures 3 plots the moduli (magnitudes) of the reflection and transmission coefficients for the simple supports. The finite cut-off frequencies, above which all wave propagates, are also marked in the figure. Thus, for the TM model, the wave motions change from *Case II* to *Case I* when $\omega > \omega_c$ ($\omega_c \cong 4$; ω_c is slightly altered by rotation speed and axial load). The results show that, at low frequencies ($\omega < 0{\cdot}1 = 3156$ rad/s), the wave reflection and transmission coefficients of the TM model agree well with those of the E-B model. However, as the frequency increases, the wave propagation characteristics of the TM model differ significantly from those of the E-B model. These differences can be explained by examining the different modes of vibration. When $\omega > \omega_c$ (in the regime of *Case I*), the vibrating motion of the TM model is dominated by shearing motion [7, 17], and hence the E-B model, which neglects the rotary inertia and shear effects, becomes inaccurate at high frequency. As discussed in reference [7], at the finite cut-off frequency, the TM shaft experiences no transverse displacement, and the cross-section of the shaft simply rotates back and forth in unison (pure shear mode).

In Figures 3(d–f), for $\beta = 0$ and $\varepsilon = 0$, the reflection and transmission coefficients of the E-B model are independent of the frequency. This is because from equation (10a), $A = 0$, and equations (9c, d) lead to a single wavenumber $\Gamma_1 = \Gamma_2$. From Appendix A, equations (A4–A7), the $\mathbf{r}$ and $\mathbf{t}$ are thus constant matrices. It is also seen that the wave reflection and transmission coefficients for both shaft models are basically independent of the rotation speed over the entire frequency range, even at high rotation speed $\beta = 0{\cdot}05 \cong 44\,600$ r.p.m. In reference [7], it is also found that β has negligible effects on the system frequency spectrum, phase velocity and group velocity. On the other hand, the

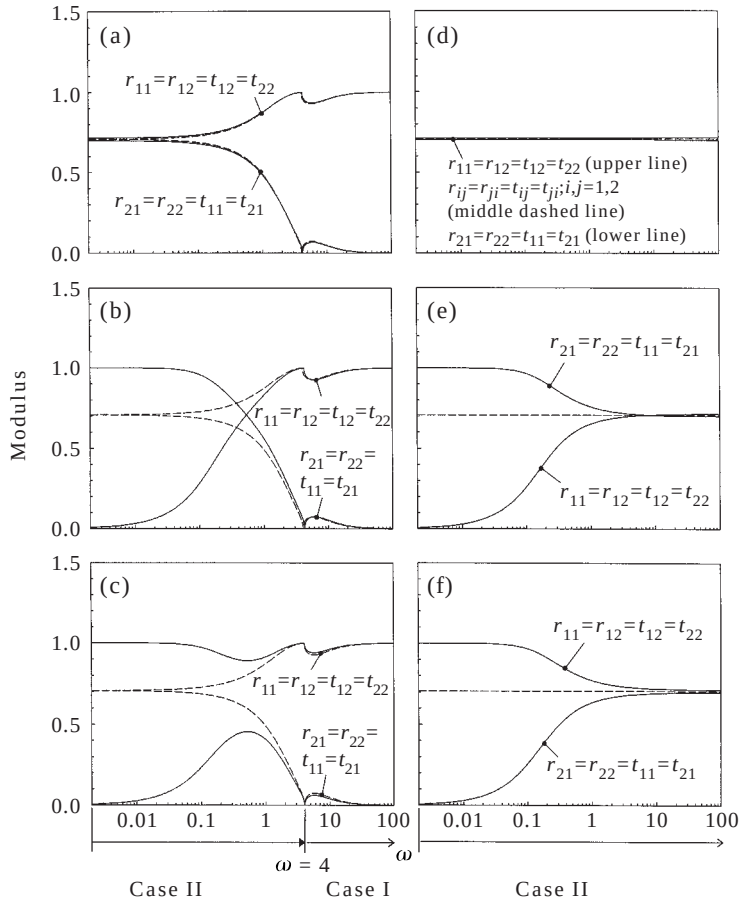

Figure 3. Wave reflection and transmission coefficients at a simple support ($k_t = \infty, k_r = c_t = c_r = m = J_m = 0$) as a function of frequency. (a)–(c) and (d)–(f) are the results for the Timoshenko and Euler–Bernoulli shaft models, respectively. The transition from one type of wave motion to another is marked for the case $\beta = \varepsilon = 0$. $\beta = \varepsilon = 0$ (——) for (a)–(f); $\beta = 0{\cdot}5$ and $\varepsilon = 0$ (——) for (a) and (d); $\beta = 0{\cdot}05$ and $\varepsilon = -0{\cdot}05$ (——) for (b) and (e); $\beta = 0{\cdot}05$ and $\varepsilon = 0{\cdot}05$ (——) for (c) and (f).

effects of the axial load are significant for both propagating and attenuating waves in the regime of *Case II*, see Figures 3(b–c). For both shaft models under compressive loads (Figures 3(b, e)), the reflection coefficient r_{11} of the incident propagating wave is reduced significantly in the regime of *Case II*, while the transmission coefficient t_{11} of the propagating wave component increases to balance the energy carried in the wave. However, the attenuating wave component t_{12} which does not carry any energy loses its transmissibility in the same amount of the reflection coefficient r_{12}. Thus, in the presence of a compressive load, most of the transmitted wave energy in *Case II* comes from the propagating component of the incident wave. Note that axial tensile loads have the reverse effect on these wave components.

Since there is no damping at the support, the incident power (Π_{inc}), reflected power (Π_{refl}) and transmitted power (Π_{tran}) in *Cases II* and *IV* are related by $\Pi_{inc} = \Pi_{refl} + \Pi_{tran} = (|r_{11}|^2 + |t_{11}|^2)\Pi_{inc}$, or $|r_{11}|^2 + |t_{11}|^2 = 1$. This relationship is confirmed by plots shown in Figure 3, where for both shaft models, $|r_{11}|$ and $|t_{11}|$ cannot exceed one. However, in the regime of *Case I*, in which all wave components propagate, the energy balance is $\Pi_{inc} = (|r_{11} + r_{21}|^2 + |t_{11} + t_{21}|^2)\Pi_{inc}$, or $\Pi_{inc} = (|r_{12} + r_{22}|^2 + |t_{12} + t_{22}|^2)\Pi_{inc}$. Together with

plots on the phase of these coefficients (not shown to reduce manuscript size), the above relationships can also be verified for wave motion of *Case I*.

3.2. WAVE REFLECTION AND TRANSMISSION AT ELASTIC SUPPORTS

Figure 4 shows the reflection and transmission coefficients for waves incident upon a support with a finite translational spring for three different spring constants. Figures 4(a, b) and (c, d) are results for the TM and E-B models, respectively. The spring constant used, $k_{t0} = 10^9$ N/m, is a typical bearing spring constant value for turbine generators. The plots show that there is no significant difference in the moduli between the two shaft models. This is because the incident wave does not experience any rotational constraint at the support, and hence the additional rotary inertia factor in the TM model makes only a small contribution to the wave motion. As the support spring constant increases, the curves for both the reflection and transmission coefficients are shifted to the right and, as the spring constant approaches infinity, these curves eventually become asymptotic to those shown in Figure 3. Note that an impedance matching ($\mathbf{r} = 0$, $\mathbf{t} = \mathbf{I}$), where all wave components are transmitted without being reflected, is found in the high frequency region for both shaft models. Thus, as the frequency increases, the characteristics of waves travelling along the shaft remain unchanged such that waves propagate through the elastic support without "resistance". It can be shown that TM has at most two impedance matching frequencies by solving $r_{11} = 0$ for real roots. The impedance mismatching ($r_{11} = 1$, $t_{11} = 0$) frequency at which the propagating wave component is completely reflected without being transmitted can also be determined from Figures 4(b, d) for the two shaft models. Note that this impedance mismatching frequency is located in the regime of *Case II*. Numerical results show, as the spring constant increases, this impedance mismatching frequency increases, but is limited to within the regime of *Case II* and can never be found in the

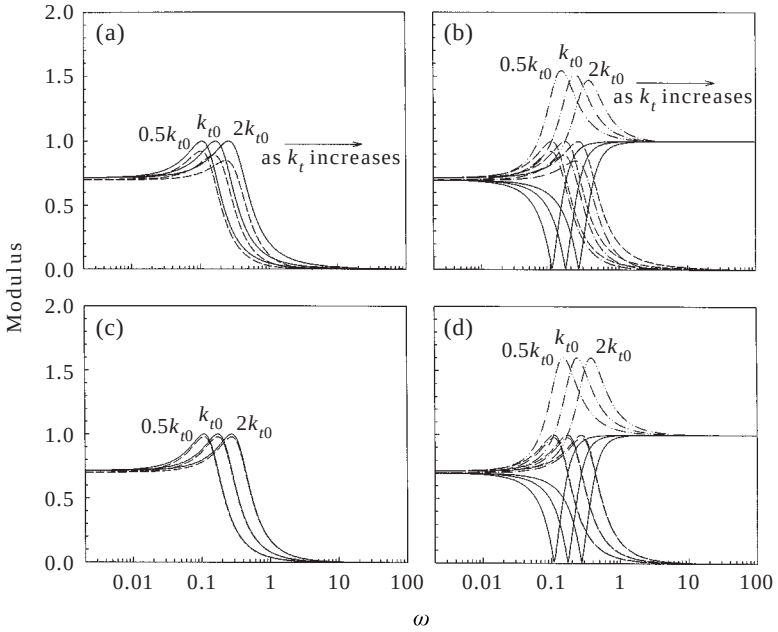

Figure 4. Wave reflection and transmission coefficients at an elastic support with a translational spring ($k_t \neq 0$, $k_r = c_t = c_r = m = J_m = 0$) as a function of frequency, $\beta = 0{\cdot}05$ and $\varepsilon = 0$. (a)–(b) and (c)–(d) are the results for the Timoshenko and Euler–Bernoulli shaft models, respectively; $r_{11} = r_{12}$ (——), $r_{21} = r_{22}$ (——) for (a) and (c); t_{11} (——), t_{12} (——), t_{21} (–·–), t_{22} (–·–) for (b) and (d).

regime of *Case I* where the shearing motion dominates the vibration of the shaft (refer to Figure 3 for the transition of types of wave motion).

Figure 5 shows the reflection and transmission coefficients for waves incident upon a support having both translational and rotational constraints. Since both translation and rotation of the cross-section are constrained at this support, the maximum of the reflection coefficient is expected to be higher than the previous case. Figures 5(a, b) and (c, d) are the results for the TM and the E-B models, respectively. The translational and rotational spring constants used in the simulation are $k_{t0} = 10^9$ N/m and $k_{r0} = 10^9$ Nm/rad, respectively. It is noted that in the regime of *Case II*, i.e., in the low frequency range, both shaft models have similar reflection characteristics, and both the reflection and transmission coefficients are not significantly affected by the rotational spring. However, as the frequency increases the effect of the rotational constraint on the wave motion becomes eminent, particularly for the TM model. As seen in Figures 5(a, c), the reflections of the attenuating wave components are significantly higher than those of the propagating wave components. Hence, when a rotating shaft has a clamped support(s) such as a journal bearing, contributions from the attenuating wave components should be included in the formulation since a significant amount of energy in the propagating component arises from the incident attenuating wave component. It is noted that the impedance matching regions seen in Figures 4(a, c) disappear when the rotational constraint is added. Moreover, the impedance mismatching frequency shown in Figures 4(b, d), which is found in the regime of *Case II*, also does not occur. At low frequency in Figures 5(b, d), there appears to be a mismatching region, but t_{11} is not exactly equal to zero. From Figures 5(a, c), it is seen that there is a frequency at which the positive propagating wave component r_{11} is zero (this frequency is slightly different for the two models). This frequency does not correspond to an impedance matching, though the propagating wave is not reflected at all but is only

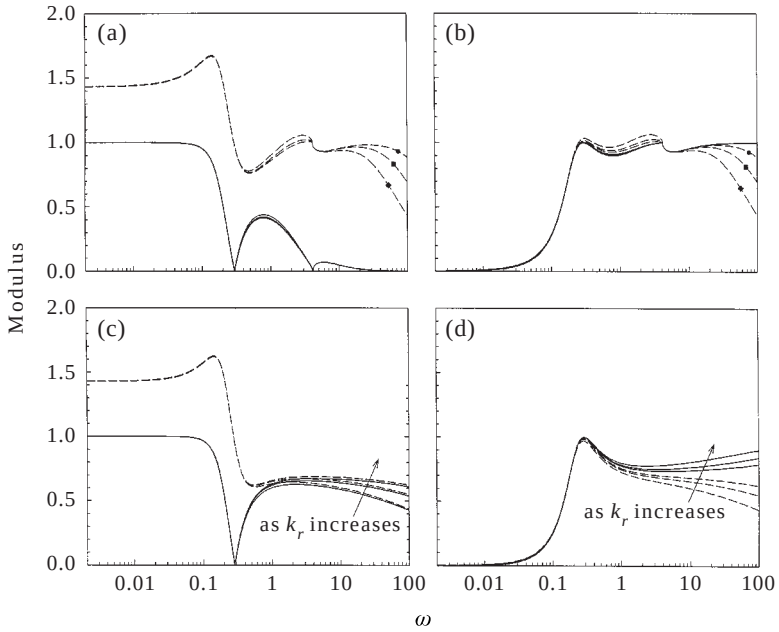

Figure 5. Wave reflection and transmission coefficients at an elastic support with translational and rotational springs ($k_t = k_{t0}$, $k_r \neq 0$, $c_t = c_r = m = J_m = 0$) as a function of frequency, $\beta = 0{\cdot}05$, $\varepsilon = 0$. (a)–(b) and (c)–(d) are results for the Timoshenko and Euler–Bernoulli shaft models, respectively; r_{11} (——), r_{12} (—), for (a) and (c); t_{11} (——), t_{12} (—) for (b) and (d); $k_r = 2k_{r0}$ (●), $k_r = k_{r0}$ (■), $k_r = 0{\cdot}5k_{r0}$ (◆).

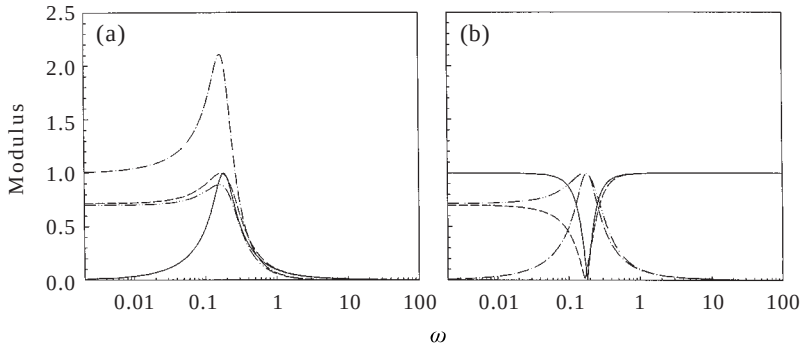

Figure 6. Wave reflection (a) and transmission (b) coefficients at an elastic support ($k_t = k_{t0}$, $k_r = c_t = c_r = m = J_m = 0$) for the Timoshenko shaft model with and without the compressive load, $\beta = 0{\cdot}05$; r_{11}, t_{11} (——), r_{12}, t_{12} (–··–) when $\varepsilon = 0$; r_{11}, t_{11} (——), r_{12}, t_{12} (–·–) when $\varepsilon = -0{\cdot}05$.

transmitted ($t_{11} = 1$). Based on other research results [18], this phenomenon likely indicates a structural *mode delocalization* in bi-coupled systems, in which vibrations on both sides of the support become strongly coupled. Further research on the vibrations of rotating shafts with intermediate supports is being pursued to confirm the mode delocalization.

Figure 6 plots the effects of axial compressive loads on the wave reflection and transmission upon a support with finite spring constant for the Timoshenko shaft model. As seen in Figure 6(a), the reflection coefficient for the incident propagating wave component r_{11} is substantially reduced in the low frequency range while the reflection coefficient for the incident attenuating wave component increases significantly. However, Figure 6(b) shows the reversed effects on the transmission coefficient. It can therefore be concluded that, when the shaft is axially strained by compressive loads, the energy contribution from the incident attenuating wave component to the energy in the reflected propagation is more significant than the strain-free situation in the low frequency range, while most of the energy in the transmitted wave derives from the incident propagating wave component.

Figure 7 plots the wave reflection and transmission coefficients along an axially compressed Timoshenko shaft model at a support with finite translational and rotational spring constants. Similar results to the previous example can be observed in terms of energy contribution from the incident attenuating wave component in the low frequency range. However, the effects of the axial compressive load on both the reflection and transmission

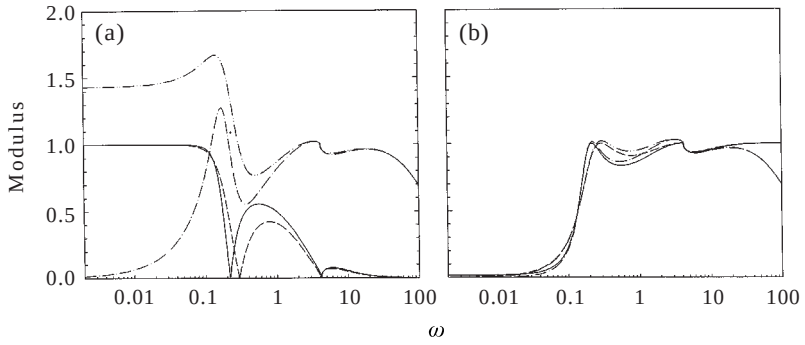

Figure 7. Wave reflection (a) and transmission (b) coefficients at an elastic support ($k_t = k_{t0}$, $k_r = k_{r0}$, $c_t = c_r = m = J_m = 0$) for the Timoshenko shaft model with and without the compressive load, $\beta = 0{\cdot}05$; r_{11}, t_{11} (——), r_{12}, t_{12} (–··–) when $\varepsilon = 0$; r_{11}, t_{11} (——), r_{12}, t_{12} (–·–) when $\epsilon = -0{\cdot}05$.

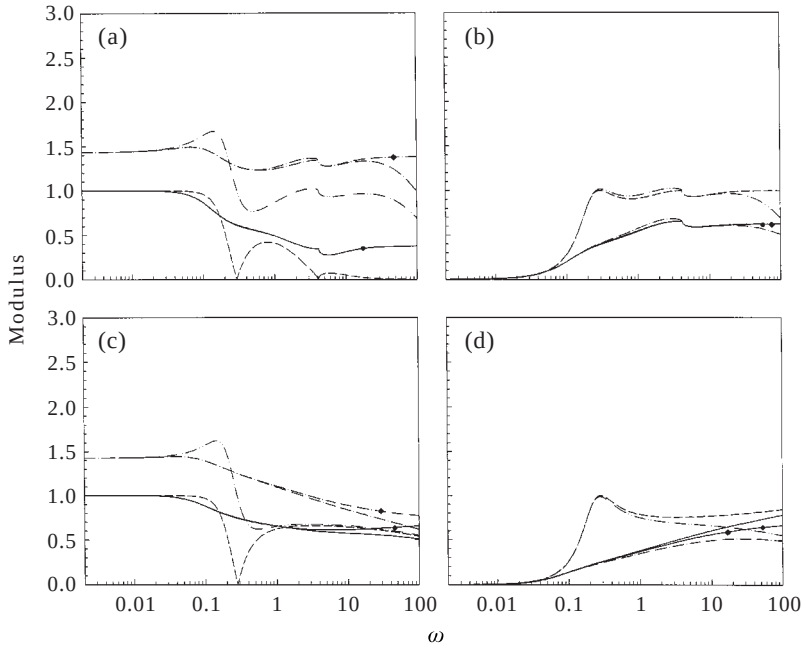

Figure 8. Wave reflection (a, c) and transmission (b, d) coefficients at an elastic support with damping ($k_t = k_{t0}$, $k_r = k_{r0}$, $m = J_m = 0$) as a function of $\beta = 0{\cdot}05$; $\varepsilon = 0$; r_{11}, t_{11} (——), r_{12}, t_{12} (–..–) when $c_t = c_r = 0$; r_{11}, t_{11} (——), r_{12}, t_{12} (–.–) when $c_t = c_{dt0}$, $c_r = 0$; r_{11}, t_{11} (—●—), r_{12}, t_{12} (—.◆—) when $c_t = c_{dt0}$, $c_r = c_{dr0}$. (a, b) and (c, d) are results for the Timoshenko and Euler–Bernoulli shaft models, respectively.

coefficients for the propagating wave component (r_{11} and t_{11}) are significantly reduced when compared to Figure 6.

3.3. WAVE REFLECTION AND TRANSMISSION AT DAMPED SUPPORTS

Figure 8 shows the effects of both translational and rotational dampers at a support with finite translational and rotational spring constants. Figures 8(a, b) and (c, d) are results for the TM and E-B models, respectively. The translational and rotational damping constants are $c_{dt0} = 2 \times 10^5$ N · s/m and $c_{dr0} = 64 \times 10^5$ N · m · s/rad, typical values for bearings in turbine generators. The curves with symbols (● and ◆) are the results when the rotational damping is included in the formulation. It is seen that $|t_{11}|$ and $|t_{12}|$ for both shaft models are significantly reduced due to the presence of damping. Moreover, because of the damping, the frequency at which $|r_{11}| = 0$ (compare with Figures 5(a, c)) no longer exists for both shaft models. Figure 8 also shows that the effects of rotational damping on the wave reflection and transmission are not significant over the entire frequency range for both shaft models. For the TM model, the effects of the rotational damping on both $|r_{11}|$ and $|t_{11}|$ are basically negligible. Since the support condition considered in this example is an actual bearing support adopted in turbine generators, it can thus be concluded that the effects of rotational damping on wave reflection and transmission are not important for practical applications. Other sets of numerical results (not presented here) also support the above finding and show that only the effects of the translational damping are important.

3.4. WAVE REFLECTION AND TRANSMISSION AT A ROTOR MASS

Consider a gear rigidly assembled to a rotating shaft. The gear is assumed to be perfectly balanced and its thickness is sufficiently small such that wave reflection and transmission

due to the geometric discontinuity between the shaft and the gear can be neglected. However, the gear does resist the translational and rotational motions of the cross-sectional element of the shaft. Figure 9 shows the reflection and transmission upon the gear when the mass m_0 and mass moment of inertia J_{m0} of the gear are 4 and 16 times that of the shaft, respectively. Not shown in Figures 9(b, d) is that $r_{ij} = 0$, $t_{12} = 0$ when $m = J_m = 0$. Like some support conditions previously discussed, the effects of the rotor mass are much more significant in the high frequency region for both models (particularly around and beyond the cut-off frequency for the TM model). In general, the rotor mass decreases the transmission and increases the reflection of the wave. At very high frequency, there is basically no wave transmission. Note that, since the geometric discontinuity between the shaft and the gear is neglected in this model, one may expect that the actual reflection for both the propagating and attenuating wave components would be higher.

4. WAVE REFLECTION AND TRANSMISSION AT A GEOMETRIC DISCONTINUITY

It is common for a rotating shaft element to have changes in cross-section, or to be joined to another shaft element by a coupling. Figure 10 shows a typical example of a discontinuous shaft model in which two shafts of differing wavenumber and diameter are joined at $Z = 0$. The subscripts l and r denote $Z = 0^-$ and $Z = 0^+$ regions, respectively. It is known that when a wave encounters a junction or a discontinuity, its wavenumber is changed. It is therefore possible that a wave on the left of the junction can be propagating, while after crossing the junction to the right side, the wave becomes attenuating. Therefore, for a Timoshenko shaft, when a wave propagates through the junction, there are mathematically nine different possible combinations of wave motions

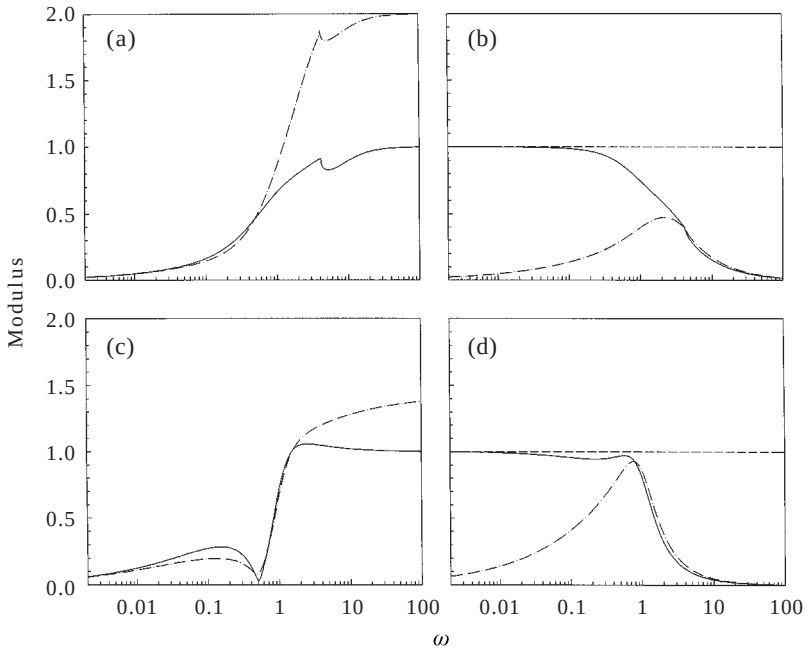

Figure 9. Wave reflection (a, c) and transmission (b, d) coefficients at a rotor mass assembled to a rotating shaft ($k_l = k_r = c_l = c_r = 0$, $m = m_0$, $J_m = J_{m0}$) as a function of frequency, $\beta = 0$, $\varepsilon = 0$; r_{11}, t_{11} (——), r_{12}, t_{12} (–·–); t_{11} (——), when $m = J_m = 0$. (a, b) and (c, d) are results for the Timoshenko and Euler–Bernoulli shaft models, respectively.

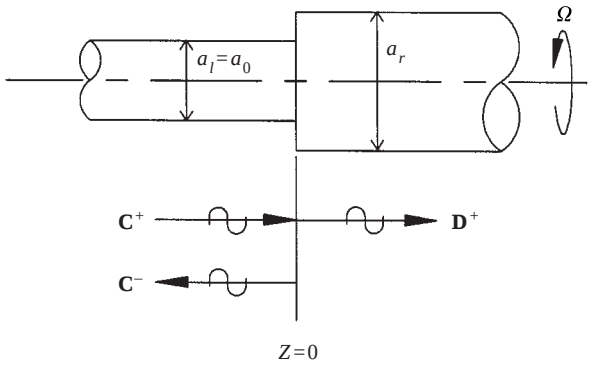

Figure 10. Wave reflection and transmission at a geometric discontinuity (*Case I*, *II* or *IV*) $A_l = (1+\alpha)\omega^2 - 2\beta\omega - 16\varepsilon'$, $A_r = (1+\alpha)\omega^2 - 2\beta\omega - (16\varepsilon_r/\sigma^2)\varepsilon_r'$), $B_l = \omega^2[\alpha\omega^2 - 2\beta\omega - 16\alpha(1+\varepsilon')]$, $B_r = \omega^2[\alpha\omega^2 - 2\beta\omega - (16\alpha/\sigma^2)\varepsilon_r']$.

to be considered depending on the values of the functions A and B on each side of the junction, as depicted in Figure 11.

For simplicity, assume that material properties such as ρ, E, and G are the same for both sides of shaft element. The geometric continuity, moment and force equilibrium conditions are applied at the junction to determine the wave reflection and transmission matrices. Results for the three most commonly encountered possibilities in the low frequency regime are listed as follows.

Case II ($A_l > 0,\ B_l < 0$)–*Case I* ($A_r > 0,\ B_r > 0$):

$$\begin{bmatrix} 1 & 1 \\ \eta_{1l} & \eta_{2l} \end{bmatrix}\mathbf{C}^+ + \begin{bmatrix} 1 & 1 \\ -\eta_{1l} & -\eta_{2l} \end{bmatrix}\mathbf{r}\mathbf{C}^+ = \begin{bmatrix} 1 & 1 \\ \eta_{1r} & \eta_{2r} \end{bmatrix}\mathbf{t}\mathbf{C}^+, \tag{37a}$$

$$\begin{bmatrix} -\mathrm{i}\Gamma_{1l}\eta_{1l} & -\Gamma_{2l}\eta_{2l} \\ \mathrm{i}(\Gamma_{1l} - \eta_{1l}) & \Gamma_{2l} - \mathrm{i}\eta_{2l} \end{bmatrix}\mathbf{C}^+ + \begin{bmatrix} -\mathrm{i}\Gamma_{1l}\eta_{1l} & -\Gamma_{2l}\eta_{2l} \\ -\mathrm{i}(\Gamma_{1l} - \eta_{1l}) & -(\Gamma_{2l} - \mathrm{i}\eta_{2l}) \end{bmatrix}\mathbf{r}\mathbf{C}^+$$

$$= \begin{bmatrix} -\mathrm{i}\sigma^4\gamma_{1r}\eta_{1r} & -\mathrm{i}\sigma^4\gamma_{2r}\eta_{2r} \\ -\mathrm{i}\sigma^2(\gamma_{1r} - \eta_{1r}) & -\mathrm{i}\sigma^2(\gamma_{2r} - \eta_{2r}) \end{bmatrix}\mathbf{t}\mathbf{C}^+; \tag{37b}$$

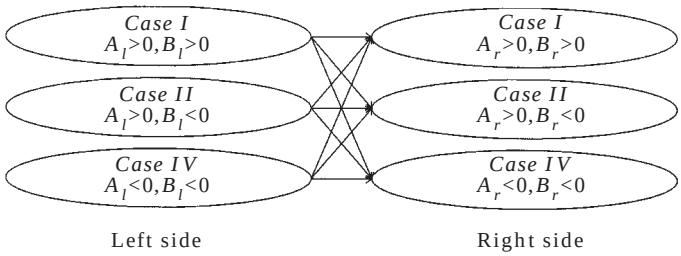

Figure 11. Nine possible combinations of wave motions at a geometric discontinuity of a cross-section of the Timoshenko shaft model. Subscripts l and r denote the left and the right side of the discontinuity, respectively.

Case II ($A_l > 0,\ B_l < 0$)–*Case II* ($A_r > 0,\ B_r < 0$):

$$\begin{bmatrix} 1 & 1 \\ \eta_{1l} & \eta_{2l} \end{bmatrix}\mathbf{C}^+ + \begin{bmatrix} 1 & 1 \\ -\eta_{1l} & -\eta_{2l} \end{bmatrix}\mathbf{rC}^+ = \begin{bmatrix} 1 & 1 \\ \eta_{1r} & \eta_{2r} \end{bmatrix}\mathbf{tC}^+, \tag{38a}$$

$$\begin{bmatrix} -\mathrm{i}\Gamma_{1l}\eta_{1l} & -\Gamma_{2l}\eta_{2l} \\ \mathrm{i}(\Gamma_{1l} - \eta_{1l}) & \Gamma_{2l} - \mathrm{i}\eta_{2l} \end{bmatrix}\mathbf{C}^+ + \begin{bmatrix} -\mathrm{i}\Gamma_{1l}\eta_{1l} & -\Gamma_{2l}\eta_{2l} \\ -\mathrm{i}(\Gamma_{1l} - \eta_{1l}) & -(\Gamma_{2l} - \mathrm{i}\eta_{2l}) \end{bmatrix}\mathbf{rC}^+$$

$$= \begin{bmatrix} -\mathrm{i}\sigma^4\Gamma_{1r}\eta_{1r} & -\sigma^4\Gamma_{2r}\eta_{2r} \\ -\mathrm{i}\sigma^2(\Gamma_{1r} - \eta_{1r}) & -\sigma^2(\Gamma_{2r} - \eta_{2r}) \end{bmatrix}\mathbf{tC}^+; \tag{38b}$$

Case II ($A_l > 0,\ B_l > 0$)–*Case IV* ($A_r < 0,\ B_r < 0$):

$$\begin{bmatrix} 1 & 1 \\ \eta_{1l} & \eta_{2l} \end{bmatrix}\mathbf{C}^+ + \begin{bmatrix} 1 & 1 \\ -\eta_{1l} & -\eta_{2l} \end{bmatrix}\mathbf{rC}^+ = \begin{bmatrix} 1 & 1 \\ \eta_{1r} & \eta_{2r} \end{bmatrix}\mathbf{tC}^+, \tag{39a}$$

$$\begin{bmatrix} -\mathrm{i}\Gamma_{1l}\eta_{1l} & -\Gamma_{2l}\eta_{2l} \\ \mathrm{i}(\Gamma_{1l} - \eta_{1l}) & \Gamma_{2l} - \mathrm{i}\eta_{2l} \end{bmatrix}\mathbf{C}^+ + \begin{bmatrix} -\mathrm{i}\Gamma_{1l}\eta_{1l} & -\Gamma_{2l}\eta_{2l} \\ -\mathrm{i}(\Gamma_{1l} - \eta_{1l}) & -(\Gamma_{2l} - \mathrm{i}\eta_{2l}) \end{bmatrix}\mathbf{rC}^+$$

$$= \begin{bmatrix} -\sigma^4\Gamma_{1r}\eta_{1r} & -\mathrm{i}\sigma^4\Gamma_{2r}\eta_{2r} \\ -\sigma^2(\Gamma_{1r} - \eta_{1r}) & -\mathrm{i}\sigma^2(\Gamma_{2r} - \eta_{2r}) \end{bmatrix}\mathbf{tC}^+; \tag{39b}$$

where σ is the diameter ratio between the shaft elements, defined as

$$\sigma = a_r / a_l. \tag{40}$$

Note that η_l's in equations (37a)–(39b) are given by equations (20a, b), (22a, b) and (24a, b) according to the type of wave motion, and the η_r's on the right side of the geometric discontinuity are modified as follows:

$$\eta_{1r} = \frac{\gamma_{1r}^2 - \omega^2}{\gamma_{1r}\,\varepsilon_r'}, \qquad \eta_{2r} = \frac{\gamma_{2r}^2 - \omega^2}{\gamma_{2r}\,\varepsilon_r'}, \quad \text{for } \textit{Case I}, \tag{41a, b}$$

$$\eta_{1r} = \frac{\Gamma_{1r}^2 - \omega^2}{\Gamma_{1r}\,\varepsilon_r'}, \qquad \eta_{2r} = \frac{\Gamma_{2r}^2 + \omega^2}{\mathrm{i}\Gamma_{2r}\,\varepsilon_r'}, \quad \text{for } \textit{Case II}, \tag{42a, b}$$

$$\eta_{1r} = \frac{\Gamma_{1r}^2 + \omega^2}{\mathrm{i}\Gamma_{1r}\,\varepsilon_r'}, \qquad \eta_{2r} = \frac{\Gamma_{2r}^2 - \omega^2}{\Gamma_{2r}\,\varepsilon_r'}, \quad \text{for } \textit{Case IV}, \tag{43a, b}$$

where

$$\varepsilon_r' = 1 + \varepsilon_r - \varepsilon_r/\alpha \quad \text{and} \quad \varepsilon_r = \varepsilon/\sigma^2. \tag{44}$$

Moreover, the wavenumbers, A and B of the shaft element on the right side of the junction are modified as follows:

$$\gamma_{1r} = \frac{1}{\sqrt{2}}(A_r + \sqrt{A_r^2 - 4B_r})^{1/2}, \qquad \gamma_{2r} = \frac{1}{\sqrt{2}}(A_r - \sqrt{A_r^2 - 4B_r})^{1/2}, \tag{45a, b}$$

$$\Gamma_{1r} = \frac{1}{\sqrt{2}}(\sqrt{A_r^2 + 4|B_r|} + |A_r^2|)^{1/2}, \qquad \Gamma_{2r} = \frac{1}{\sqrt{2}}(\sqrt{A_r^2 + 4|B_r|} - |A_r^2|)^{1/2}, \tag{45c, d}$$

where

$$A_r = (1+\alpha)\omega^2 - 2\beta\omega - \frac{16\varepsilon_r}{\sigma^2}\left(1+\varepsilon_r - \frac{\varepsilon_r}{\alpha}\right), \tag{46a}$$

$$B_r = \omega^2\left[\alpha\bar{\omega}^2 - 2\beta\bar{\omega} - \frac{16\alpha}{\sigma^2}(1+\varepsilon_r)\left(1+\varepsilon_r - \frac{\varepsilon_r}{\alpha}\right)\right]. \tag{46b}$$

Corresponding results for the simple E-B shaft model are listed in Appendix B.

Figures 12–15 show some representative examples of wave reflection and transmission upon the geometric discontinuity. In Figures 12 and 13, the thick and thin curves represent results for the TM and E-B models, respectively. The second graph in each figure shows the changes of A_l, B_l, A_r and B_r, and how wave solutions on both sides of the discontinuity change as the frequency increases for the TM model. In general, the wave reflection and transmission for the E-B model are frequency independent except when the shaft is axially strained, while the wave propagation characteristics for the TM model are strongly dependent on the frequency.

Comparing Figures 12 and 13, it is noted that, for both shaft models, the average reflection and transmission rates for $\sigma = 0{\cdot}8$ are higher than those for $\sigma = 1{\cdot}2$, especially for the attenuating wave components. These results imply that incident attenuating waves contribute more energy to propagating waves at the discontinuity when the waves travel from a smaller to a larger cross-section. In particular, it is noted that the transmissibility of the attenuating wave t_{12} has a strong dependency on the direction of propagation. Note also that the differences between the two shaft models are more pronounced when $\sigma = 0{\cdot}8$. It is clearly seen from the figures that when B_l and B_r change from negative to positive, both reflection and transmission coefficients experience a sharp jump or drop at the finite cut-off frequencies, due to changes in the types of wave motion. In the frequency region ($B_l > 0$ and $B_r < 0$) located between the two cut-off frequencies in Figure 12, the wave

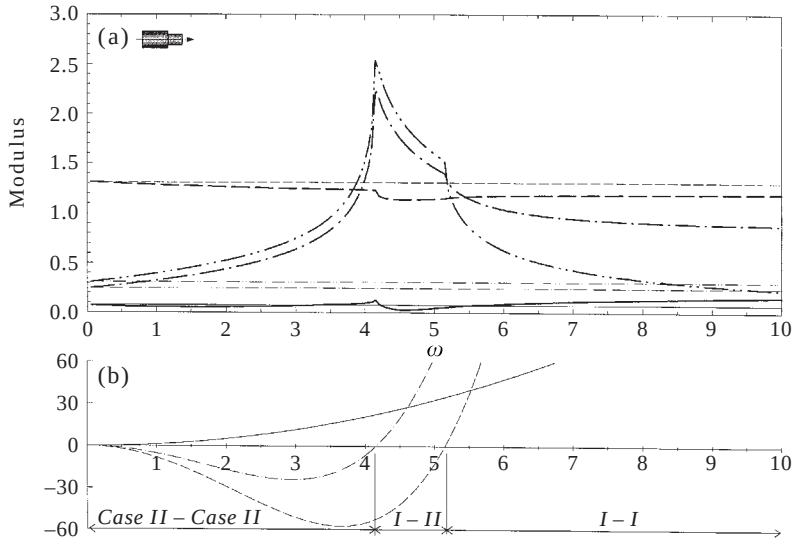

Figure 12. Reflection and transmission of waves incident upon a change in the cross-section, $\sigma = 0{\cdot}8$, $\beta = 0{\cdot}05$, $\varepsilon = 0$. Thick and thin curves represent results for the Timoshenko and Euler–Bernoulli shaft models, respectively; r_{11} (——), r_{12} (–·–), t_{11} (——), t_{12} (–··–) for (a); B_l (–.–), B_r (——), $A_l = A_r$ (——) for (b).

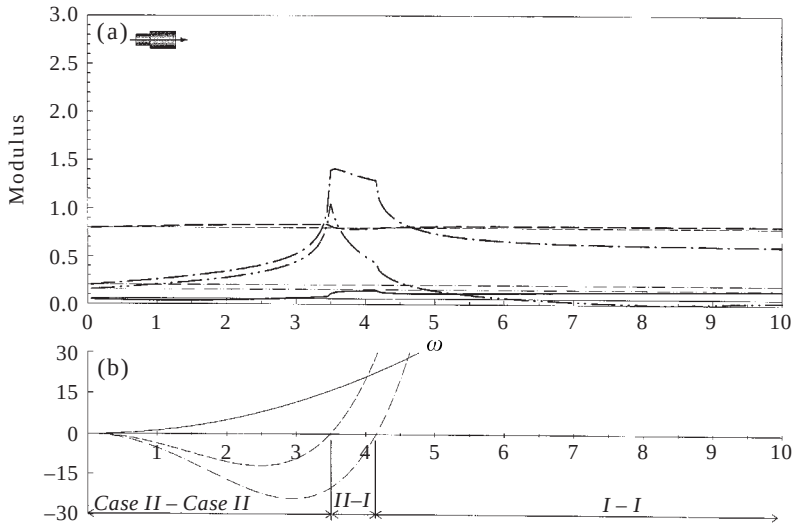

Figure 13. Reflection and transmission of waves incident upon a change in the cross-section, $\sigma = 1{\cdot}2$, $\beta = 0{\cdot}05$, $\varepsilon = 0$. Thick and thin curves represent results for the Timoshenko and Euler–Bernoulli shaft models, respectively; r_{11} (——), r_{12} (–·–), t_{11} (——), t_{12} (–··–) for (a); B_l (–•–), B_r (——), $A_l = A_r$ (——) for (b).

motion on the left side of the junction is governed by the wave solution of *Case I* since all wave components are propagating at a frequency larger than the cut-off frequency, while the wave motion on the right side of the junction is governed by the wave solution of *Case II*. Thus, for $\sigma = 0{\cdot}8$, some of the propagating wave components on the left side of the shaft element cannot propagate as they pass the discontinuity, and become attenuating. A similar, but converse conclusion can be drawn for the frequency region ($B_r > 0$, $B_l < 0$) when $\sigma = 1{\cdot}2$, as shown in Figure 13. The results of Figures 12 and 13 show that, for different system parameters σ, β and ε and at any given frequency, the types of wave motion on each side of the discontinuity can be different, as depicted in Figure 11.

From equations (41a)–(43b), it is seen that when the Timoshenko shaft is axially strained and ω is not sufficiently large, the wavenumber (hence wave propagation characteristics) depends strongly on the cross-section ratio σ. Figure 14 shows the effects of the axial load on the wave reflection and transmission, which are mostly limited to the relatively low frequency region. In Figures 14(a, b), when the shaft is axially compressed ($\varepsilon = -0{\cdot}05$), the reflection and transmission due to the incident attenuating wave component decrease for both $\sigma < 1$ (plot (a)) and $\sigma > 1$ (plot (b)). However, the transmission t_{11} due to an incident propagating wave decreases significantly for $\sigma = 0{\cdot}8$ and increases for $\sigma = 1{\cdot}2$ at low frequency.

Effects of the axialload on the wave reflection and transmission are more significant when the shaft is compressed (Figures 14(a, b)) than when it is under tension (Figures 14(c, d)). This is because the wavenumbers of both the propagating and attenuating wave components are only slightly changed. It is also noted that, in the low frequency range, the wave solution of *Case IV* governs the wave motions on both sides of the discontinuity, and the wave components which have a large wavenumber (Γ_1) attenuate, while wave components with a small wavenumber (Γ_2) propagate along the waveguide as long as A remains negative.

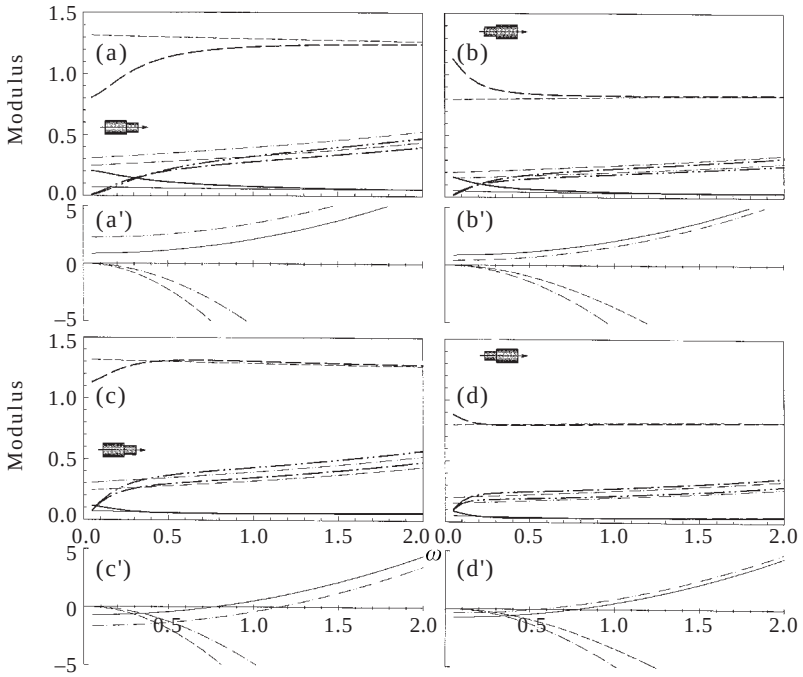

Figure 14. Reflection and transmission of waves incident upon a change in the cross-section for the Timoshenko shaft model, $\beta = 0{\cdot}05$; (a) $\sigma = 0{\cdot}8$, $\varepsilon = -0{\cdot}05$; (b) $\sigma = 1{\cdot}2$, $\varepsilon = -0{\cdot}05$; (c) $\sigma = 0{\cdot}8$, $\varepsilon = 0{\cdot}05$; (d) $\sigma = 1{\cdot}2$, $\varepsilon = 0{\cdot}05$. Thin and thick curves represent the results when $\varepsilon = 0$ and $\epsilon \neq 0$, respectively; r_{11} (——), r_{12} (–·–), t_{11} (——), t_{12} (–···–) for (a)–(d); A_l (——), A_r (–···–), B_l(–·–), B_r (——) for (a′)–(d′).

5. WAVE REFLECTION AT BOUNDARIES

When a wave is incident upon a boundary, it is only reflected because no waveguide exists beyond the boundary. Consider an arbitrary boundary condition with translational and rotational spring constraints, dampers and a rotor mass, as shown in Figure 15. The reflection matrix at the boundary is derived for each case. Applying the same non-dimensional parameters employed in section 3, and by imposing the force and moment balances at the boundary, which can be deduced by eliminating M^+ and V^+ in equations (27a, b),

$$M^- = k_r\,\psi + c_r\,\dot{\psi} + J_m\,\ddot{\psi}, \qquad -V^- = k_t\,u + c_t\,\dot{u} + m\ddot{u}, \tag{47a, b}$$

the reflection matrix for each case is determined.

Case I ($A > 0,\ B > 0$):

$$\mathbf{r} = \begin{bmatrix} \eta_1(\mathrm{i}\gamma_1 - \Sigma_m) & \eta_2(\mathrm{i}\gamma_2 - \Sigma_m) \\ \mathrm{i}(\gamma_1 - \eta_1) + \Sigma_s & \mathrm{i}(\gamma_2 - \eta_2) + \Sigma_s \end{bmatrix}^{-1} \begin{bmatrix} -\eta_1(\mathrm{i}\gamma_1 + \Sigma_m) & -\eta_2(\mathrm{i}\gamma_2 + \Sigma_m) \\ \mathrm{i}(\gamma_1 - \eta_1) - \Sigma_s & \mathrm{i}(\gamma_2 - \eta_2) - \Sigma_s \end{bmatrix}; \tag{48}$$

Case II ($A > 0,\ B < 0$);

$$\mathbf{r} = \begin{bmatrix} \eta_1(\mathrm{i}\Gamma_1 - \Sigma_m) & \eta_2(\mathrm{i}\Gamma_2 - \Sigma_m) \\ \mathrm{i}(\Gamma_1 - \eta_1) + \Sigma_s & (\Gamma_2 - \mathrm{i}\eta_2) + \Sigma_s \end{bmatrix}^{-1} \begin{bmatrix} -\eta_1(\mathrm{i}\Gamma_1 + \Sigma_m) & -\eta_2(\Gamma_2 + \Sigma_m) \\ \mathrm{i}(\Gamma_1 - \eta_1) - \Sigma_s & (\Gamma_2 - \mathrm{i}\eta_2) - \Sigma_s \end{bmatrix}; \tag{49}$$

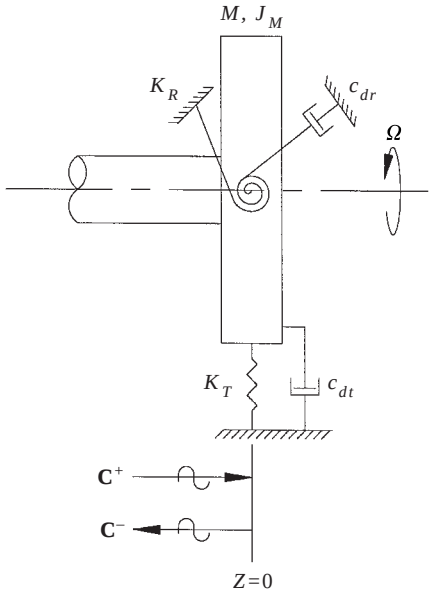

Figure 15. Wave reflection upon a general boundary for (*Case II*): $u^-(z) = C_{u1}^+ e^{-i\Gamma_1 z} + C_{u1}^- e^{i\Gamma_1 z} + C_{u2}^+ e^{-\Gamma_2 z} + C_{u2}^- e^{\Gamma_2 z}$.

Case IV ($A < 0,\ B < 0$):

$$\mathbf{r} = \begin{bmatrix} \eta_2(i\Gamma_2 - \Sigma_m) & \eta_1(\Gamma_1 - \Sigma_m) \\ i(\Gamma_2 - \eta_2) + \Sigma_s & (\Gamma_1 - i\eta_1) + \Sigma_s \end{bmatrix}^{-1} \begin{bmatrix} -\eta_2(i\Gamma_2 + \Sigma_m) & -\eta_1(\Gamma_1 + \Sigma_m) \\ i(\Gamma_2 - \eta_2) - \Sigma_s & (\Gamma_1 - i\eta_1) - \Sigma_s \end{bmatrix}; \quad (50)$$

where the η's in the above equations have been defined in equations (20a, b), (22a, b) and (24a, b) and

$$\Sigma_m = k_r + ic_r\omega - J_m\omega^2 \quad \text{and} \quad \Sigma_s = k_t + ic_t\omega - m\omega^2. \quad (51a, b)$$

The corresponding results for the simple E-B shaft model are listed in Appendix C. By specifying the parameters in the reflection matrix $\mathbf{r}$, results for three typical boundary conditions (simple support, clamped support, and free end) can be obtained.

Simple support ($k_t = \infty,\ k_r = m = c_t = c_r = J_m = 0$)

$$\mathbf{r} = \begin{bmatrix} -1 & 0 \\ 0 & -1 \end{bmatrix} \text{ for } \textit{Cases I, III and IV}. \quad (52)$$

Clamped support ($k_t = \infty,\ k_r = \infty,\ m = c_t = c_r = J_m = 0$)

$$\mathbf{r} = \frac{1}{\eta_1 - \eta_2} \begin{bmatrix} \eta_1 + \eta_2 & 2\eta_2 \\ -2\eta_1 & -(\eta_1 + \eta_2) \end{bmatrix} \text{ for } \textit{Case I}, \quad (53a)$$

$$\mathbf{r} = \frac{1}{\eta_1 - \eta_2} \begin{bmatrix} \eta_1 + \eta_2 & 2\eta_2 \\ -2\eta_1 & -(\eta_1 + \eta_2) \end{bmatrix} \text{ for } \textit{Case II}, \quad (53b)$$

$$\mathbf{r} = \frac{1}{\eta_1 - \eta_2} \begin{bmatrix} -(\eta_1 + \eta_2) & -2\eta_2 \\ 2\eta_1 & (\eta_1 + \eta_2) \end{bmatrix} \text{ for } \textit{Case IV}. \quad (53c)$$

Free end ($k_t = k_r = m = c_t = c_r = J_m = 0$ and $\epsilon = 0$)

$$\mathbf{r} = \frac{1}{\Delta_I}\begin{bmatrix} \eta_1\eta_2(\gamma_1+\gamma_2) - \gamma_1\gamma_2(\eta_1+\eta_2) & 2\eta_2\gamma_2(\eta_2-\gamma_2) \\ -2\eta_1\gamma_1(\eta_1-\gamma_1) & -\eta_1\eta_2(\gamma_1+\gamma_2) + \gamma_1\gamma_2(\eta_1+\eta_2) \end{bmatrix}, \tag{54a}$$

where $\Delta_I = \eta_1\eta_2(\gamma_2-\gamma_1) + \gamma_1\gamma_2(\eta_1-\eta_2)$ for *Case I*;

$$\mathbf{r} = \frac{1}{\Delta_{II}}\begin{bmatrix} -\eta_1\eta_2(\mathrm{i}\gamma_1+\gamma_2) + \gamma_1\gamma_2(\eta_1+\eta_2) & 2\mathrm{i}\eta_2\gamma_2(\mathrm{i}\eta_2-\gamma_2) \\ 2\mathrm{i}\eta_1\gamma_1(\eta_1-\gamma_1) & \eta_1\eta_2(\mathrm{i}\gamma_1+\gamma_2) - \gamma_1\gamma_2(\eta_1+\eta_2) \end{bmatrix}, \tag{54b}$$

where $\Delta_{II} = \eta_1\eta_2(\mathrm{i}\gamma_1-\gamma_2) - \gamma_1\gamma_2(\eta_1-\eta_2)$ for *Case II*;

$$\mathbf{r} = \frac{1}{\Delta_{IV}}\begin{bmatrix} \eta_1\eta_2(\gamma_1+\mathrm{i}\gamma_2) - \gamma_1\gamma_2(\eta_1+\eta_2) & 2\eta_1\gamma_1(\eta_1+\mathrm{i}\gamma_1) \\ -2\mathrm{i}\eta_2\gamma_2(\eta_2-\gamma_2) & -\eta_1\eta_2(\gamma_1+\mathrm{i}\gamma_2) + \gamma_1\gamma_2(\eta_1+\eta_2) \end{bmatrix}, \tag{54c}$$

where $\Delta_{IV} = \eta_1\eta_2(\gamma_2-\mathrm{i}\gamma_2) - \gamma_1\gamma_2(\eta_1-\eta_2)$ for *Case IV*.

6. APPLICATIONS

The reflection and transmission matrices for waves incident upon a general point support or a change in cross-section can be combined with the transfer matrix method to analyse the free vibration of a rotating Timoshenko shaft with multiple supports and discontinuities, and general boundary conditions. The basic idea of this technique has been shown in reference [6]. However, due to the complex wave motions in the Timoshenko shaft model, such as the frequency dependency of the wave reflection and transmission at a cross-section change, it is important to apply the proper reflection and transmission matrices consistent with the values of A and B on both sides of the discontinuity, particularly when numerical calculations are performed. Consider for example the free vibration problem of the rotating Timoshenko shaft model shown in Figure 16. Denoting $\mathbf{R}$ as a reflection matrix which relates the amplitudes of negative and positive travelling waves at a discontinuity, and defining $\mathbf{T}_i$ as the field transfer matrix which relates the wave amplitudes by

$$\mathbf{C}^+(z_0+z) = \mathbf{T}\mathbf{C}^+(z_0), \qquad \mathbf{C}^-(z_0+z) = \mathbf{T}^{-1}\mathbf{C}^-(z_0), \tag{55}$$

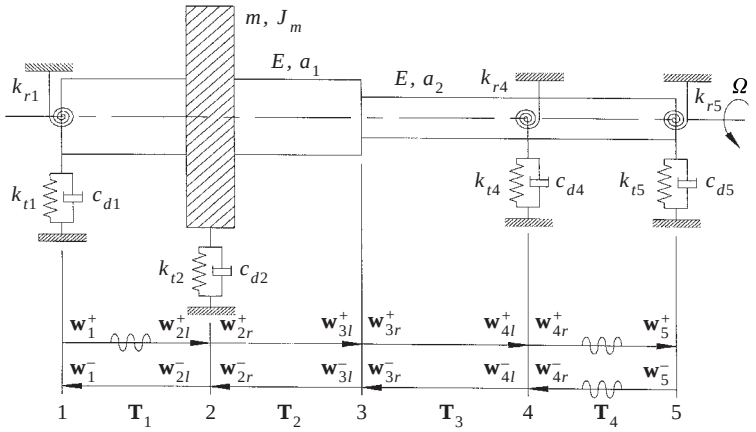

Figure 16. An example of a rotating shaft with multiple supports and discontinuities.

the following relations can be found.

$$\mathbf{w}_5^- = \mathbf{R}_5\,\mathbf{w}_5^+, \qquad (\mathbf{R}_5 = \mathbf{r}_5); \tag{56a}$$

$$\mathbf{w}_{i\mu}^- = \mathbf{R}_{i\mu}\,\mathbf{w}_{i\mu}^+, \tag{56b}$$

where $i = 2, 3, 4$ (station number), $\mu =$ left (l) or right (r);

$$\mathbf{w}_1^- = \mathbf{T}_1\,\mathbf{w}_{2l}^-, \qquad \mathbf{w}_1^+ = \mathbf{r}_1\,\mathbf{w}_1^-, \qquad \mathbf{w}_{2l}^+ = \mathbf{T}_1\,\mathbf{w}_1^+, \tag{56c–e}$$

where in equation (56b),

$$\mathbf{R}_{ir} = \mathbf{T}_i\,\mathbf{R}_{i+1,l}\,\mathbf{T}_i, \qquad \mathbf{R}_{il} = \mathbf{r}_i + \mathbf{t}_i\,(\mathbf{R}_{ir}^{-1} - \mathbf{r}_i)^{-1}\mathbf{t}_i. \tag{56f}$$

Solving the above matrix equations gives

$$(\mathbf{r}_1\,\mathbf{T}_1\,\mathbf{R}_{2l}\,\mathbf{T}_1 - \mathbf{I})\mathbf{w}_1^+ = 0, \tag{57}$$

where each element of the matrix is a function of two different wavenumbers and the frequency ω. For non-trivial solutions, the natural frequencies are obtained from the characteristic equation

$$\text{Det}\,[(\mathbf{r}_1\,\mathbf{T}_1\,\mathbf{R}_{2l}\,\mathbf{T}_1 - \mathbf{I})] = 0. \tag{58}$$

Numerical difficulties may arise in evaluating the inverses of matrices when wavenumbers are extremely small or span lengths are very long. A modified wave approach proposed in reference [19] circumvents this difficulty. However, in practical applications, such conditions do not exist. The proposed wave analysis technique can be applied to the study of structural mode localization in disordered rotating system. The dynamics of such a system will be addressed in another paper.

7. SUMMARY AND CONCLUSIONS

In modern high speed rotating shaft applications, it is common that a shaft has multiple intermediate supports and discontinuities such as bearings, rotor masses, and changes in cross-sections. In many cases, the ratio of the shaft diameter to its length between consecutive supports is large, and the Timoshenko model (TM) is needed to accurately account for the shear and rotary inertia effects. In this paper, the wave propagation in a rotating, axially strained Timoshenko shaft model with multiple discontinuities is examined. The effect of the static axial deformation due to an axial load is also included in the model. Based on results from reference [7], there are four possible types of wave motions (*Cases I*, *II*, *III* and *IV*) in the Timoshenko shaft, as shown by equations (5a)–(8b). In practice, *Case III* does not occur and is excluded in the analysis. For each case, the wave reflection and transmission matrices are derived for a shaft under various support and boundary conditions. Results are compared with those obtained by using the simple Euler–Bernoulli model (E-B) and are summarized as follows. (1) In general, the two shaft models show good agreement in the low frequency range where the wave motion is governed by *Cases II* and *IV*. However, at high frequencies, the types of wave motion and propagation characteristics for the TM and E-B models are very different. (2) The effects of shaft rotation on the wave reflection and transmission are negligible over the entire frequency range and even at high speed (up to 44 600 r.p.m.). While the effects of the axial load are significant, especially in the low frequency range. (3) When waves are incident at supports with only translational springs, differences in the results between the TM and E-B models are small, and there exist frequency regions of impedance matching and an impedance mismatching frequency (limited to within the regime of *Case II*). The

impedance matching and mismatching disappear when a rotational spring is added to the support. Instead, there is a frequency at which $|r_{11}| = 0$ and $|t_{11}| = 1$, and vibrations on both sides of the support become strongly coupled. This (delocalization) phenomenon suggests further research on the vibrations of constrained multi-span beams. When there is damping at the support, the frequency at which $|r_{11}| = 0$ does not occur. Moreover, effects of translational damping on the wave propagation are more significant at high frequency, especially for the TM model, however effects of rotational damping are not significant over the entire frequency range. (4) Contributions of attenuating wave components to the energy in the reflected and transmitted waves are significant when the shaft is axially strained and when the support has a rotational constraint. Thus, attenuating waves should be included in the formulation. (5) Unlike the spring supports, in which waves are easily transmitted at high frequency, the rotor mass support diminishes the wave transmission as the frequency increases. (6) When waves are incident at a geometric discontinuity such as a change in the cross-section, there are nine possible combinations of wave motions on both sides of the discontinuity. It is shown that differences of the results between the TM and E-B models depend on the diameter ratio (and hence the direction of the wave incidence). Moreover, incident attenuating waves contribute more energy to propagating waves at the discontinuity when the waves travel from a smaller to a larger cross-section. When the shaft is axially strained, the effects of the load on the wave propagation are primarily limited to the low frequency range.

The reflection and transmission matrices are combined with the transfer matrix method to provide a systematic solution method to analyse the free vibration of a multi-span, rotating shaft. Since the procedure involves only 2×2 (while including the near-field effects already), strenuous computations associated with large-order matrices are eliminated.

ACKNOWLEDGMENTS

The authors wish to acknowledge the support of the National Science Foundation and the Institute of Manufacturing Research of Wayne State University for this research work.

REFERENCES

1. Y. K. Lin 1962 *International Journal of Mechanical Sciences* **4**, 409–423. Free vibrations of a continuous beam on elastic supports.
2. K. F. Graff 1975 *Wave Motion in Elastic Solids*. Ohio State University Press.
3. L. Cremer, M. Heckl and E. E. Ungar 1973 *Structure-Borne Sound*. Berlin: Springer-Verlag.
4. F. Fahy 1985 *Sound and Structural Vibration*. New York: Academic Press.
5. D. J. Mead 1994 *Journal of Sound and Vibration* **171**, 695–702. Waves and modes in finite beams: application of the phase-closure principle.
6. B. R. Mace 1984 *Journal of Sound and Vibration* **97**, 237–246. Wave reflection and transmission in beams.
7. B. Kang and C. A. Tan 1998 *Journal of Sound and Vibration* **213,** 467–482. Elastic wave motions in an axially strained, infinitely long rotating Timoshenko shaft.
8. R. P. S. Han and J. W.-Z. Zu 1992 *Journal of Sound and Vibration* **156**, 1–16. Modal analysis of rotating shafts: a body-fixed axis formulation approach.
9. J. W.-Z. Zu and R. P. S. Han 1992 *Transactions of the American Society of Mechanical Engineers*, *Journal of Applied Mechanics* **59**, 197–204. Natural frequencies and normal modes of a spinning Timoshenko beam with general boundary conditions.
10. R. Katz, C. W. Lee, A. G. Ulsoy and R. A. Scott 1988 *Journal of Sound and Vibration* **122**, 131–148. The dynamic response of a rotating shaft subject to a moving load.
11. C. A. Tan and W. Kuang 1995 *Journal of Sound and Vibration* **183**, 451–474. Vibration of a rotating discontinuous shaft by the distributed transfer function method.

12. A. Argento and R. A. Scott 1995 *Wave Motion* **21**, 67–74. Elastic wave propagation in a Timoshenko beam spinning about its longitudinal axis.
13. F. M. Dimentberg 1961 *Flexural Vibrations of Rotating Shafts*. London: Butterworths.
14. A. D. Dimarogonas and S. A. Paipeties 1983 *Analytical Method in Rotor Dynamics*. New York: Applied Science.
15. C. W. Lee 1993 *Vibration Analysis of Rotors*. Dordrecht, The Netherlands: Kluwer Academic Publishers.
16. S. H. Choi, C. Pierre and A. G. Ulsoy 1992 *Journal of Vibration and Acoustics* **114**, 249–259. Consistent modelling of rotating Timoshenko shafts subject to axial loads.
17. G. R. Bhashyam and G. Prathap 1981 *Journal of Sound and Vibration* **76**, 407–420. The second frequency spectrum of Timoshenko beams.
18. C. H. Riedel and C. A. Tan 1997 *Proceedings of ASME Biennial Conference on Mechanical Vibration and Noise*, *Paper No. DETC*97/*VIB*-3951. Mode localization and delocalization in constrained strings and beams.
19. Y. Yong and Y. K. Lin 1989 *Journal of Sound and Vibration* **129**, 99–118. Propagation of decaying waves in periodic and piecewise periodic structures of finite length.

APPENDIX A: MATRIX EQUATIONS FOR EULER–BERNOULLI MODEL, GENERALIZED SUPPORT

The reflection and transmission matrices for a wave incident upon a generalized support for the simple E-B shaft model can be obtained by solving the following sets of matrix equations.

Case II ($A > 0,\ B < 0$):

$$\begin{bmatrix} 1 & 1 \\ -\mathrm{i}\Gamma_1 & -\Gamma_2 \end{bmatrix}\mathbf{C}^+ + \begin{bmatrix} 1 & 1 \\ \mathrm{i}\Gamma_1 & \Gamma_2 \end{bmatrix}\mathbf{r}\mathbf{C}^+ = \begin{bmatrix} 1 & 1 \\ -\mathrm{i}\Gamma_1 & -\Gamma_2 \end{bmatrix}\mathbf{t}\mathbf{C}^+, \tag{A1a}$$

$$\begin{bmatrix} -\Gamma_1^2 & \Gamma_2^2 \\ \mathrm{i}\Gamma_1^3 & -\Gamma_2^3 \end{bmatrix}\mathbf{C}^+ + \begin{bmatrix} -\Gamma_1^2 & \Gamma_2^2 \\ -\mathrm{i}\Gamma_1^3 & \Gamma_2^3 \end{bmatrix}\mathbf{r}\mathbf{C}^+$$

$$= \begin{bmatrix} -\Gamma_1^2 + \mathrm{i}\Gamma_1(k_r + \mathrm{i}c_r\,\omega - J_m\,\omega^2) & \Gamma_2^2 + \Gamma_2(k_r + \mathrm{i}c_r\,\omega - J_m\,\omega^2) \\ (k_t - m\omega^2) + \mathrm{i}(c_t\,\omega + \Gamma_1^3) & (k_t - m\omega^2 - \Gamma_2^3) + \mathrm{i}c_t\,\omega \end{bmatrix}\mathbf{t}\mathbf{C}^+; \tag{A1b}$$

Case IV ($A < 0,\ B < 0$):

$$\begin{bmatrix} 1 & 1 \\ -\mathrm{i}\Gamma_2 & -\Gamma_1 \end{bmatrix}\mathbf{C}^+ + \begin{bmatrix} 1 & 1 \\ \mathrm{i}\Gamma_2 & \Gamma_1 \end{bmatrix}\mathbf{r}\mathbf{C}^+ = \begin{bmatrix} 1 & 1 \\ -\mathrm{i}\Gamma_2 & -\Gamma_1 \end{bmatrix}\mathbf{t}\mathbf{C}^+, \tag{A2a}$$

$$\begin{bmatrix} -\Gamma_2^2 & \Gamma_1^2 \\ \mathrm{i}\Gamma_2^3 & -\Gamma_1^3 \end{bmatrix}\mathbf{C}^+ + \begin{bmatrix} -\Gamma_2^2 & \Gamma_1^2 \\ -\mathrm{i}\Gamma_2^3 & \Gamma_1^3 \end{bmatrix}\mathbf{r}\mathbf{C}^+$$

$$= \begin{bmatrix} -\Gamma_2^2 + \mathrm{i}\Gamma_2(k_r + \mathrm{i}c_r\,\omega - J_m\,\omega^2) & \Gamma_1^2 + \Gamma_1(k_r + \mathrm{i}c_r\,\omega - J_m\,\omega^2) \\ (k_t - m\omega^2) + \mathrm{i}(c_t\,\omega + \Gamma_2^3) & (k_t - m\omega^2 - \Gamma_1^3) + \mathrm{i}c_t\,\omega \end{bmatrix}\mathbf{t}\mathbf{C}^+; \tag{A2b}$$

where the following non-dimensional parameters are employed:

$$k_t=\frac{K_t a_0^3}{EI},\quad k_r=\frac{K_r a_0}{EI},\quad c_t=\frac{c_{dt} c_0 a_0^2}{EI},\quad c_r=\frac{c_{dr} c_0}{EI},\quad m=\frac{Ma_0}{\rho I}\quad J_m=\frac{J_M c_0^2}{EI}\quad \text{and}\quad c_0=\sqrt{\frac{E}{\rho}}. \tag{A3}$$

For simple and clamped supports, the reflection and transmission matrices are listed as follows.

Simple support ($k_t=\infty,\ k_r=m=c_t=c_r=J_m=0$)

Case II ($A>0,\ B<0$):

$$\mathbf{r}=\frac{1}{\mathrm{i}\Gamma_1-\Gamma_2}\begin{bmatrix}\Gamma_2 & \Gamma_2\\ -\mathrm{i}\Gamma_1 & -\mathrm{i}\Gamma_1\end{bmatrix},\qquad \mathbf{t}=\frac{1}{\mathrm{i}\Gamma_1-\Gamma_2}\begin{bmatrix}\mathrm{i}\Gamma_1 & \Gamma_2\\ -\mathrm{i}\Gamma_1 & -\Gamma_2\end{bmatrix}; \tag{A4a, b}$$

Case IV ($A<0,\ B<0$):

$$\mathbf{r}=\frac{1}{\mathrm{i}\Gamma_1+\Gamma_2}\begin{bmatrix}-\mathrm{i}\Gamma_1 & -\mathrm{i}\Gamma_1\\ -\Gamma_2 & -\Gamma_2\end{bmatrix},\qquad \mathbf{t}=\frac{1}{\mathrm{i}\Gamma_1+\Gamma_2}\begin{bmatrix}\Gamma_2 & -\mathrm{i}\Gamma_1\\ -\Gamma_2 & \mathrm{i}\Gamma_1\end{bmatrix}. \tag{A5a, b}$$

Clamped support ($k_t=\infty,\ k_4=\infty,\ m=c_t=c_r=J_m=0$); $\mathbf{t}=0$

Case II ($A>0,\ B<0$):

$$\mathbf{r}=\frac{1}{\mathrm{i}\Gamma_1-\Gamma_2}\begin{bmatrix}\mathrm{i}\Gamma_1+\Gamma_2 & 2\Gamma_2\\ -2\mathrm{i}\Gamma_1 & -(\mathrm{i}\Gamma_1+\Gamma_2)\end{bmatrix}; \tag{A6}$$

Case IV ($A<0,\ B<0$):

$$\mathbf{r}=\frac{1}{\mathrm{i}\Gamma_1+\Gamma_2}\begin{bmatrix}-(\mathrm{i}\Gamma_1-\Gamma_2) & -\mathrm{i}2\Gamma_1\\ -2\Gamma_2 & \mathrm{i}\Gamma_1-\Gamma_2\end{bmatrix}. \tag{A7}$$

APPENDIX B: MATRIX EQUATIONS FOR EULER–BERNOULLI MODE, CROSS-SECTIONAL CHANGE

The reflection and transmission matrices for a wave incident upon a cross-sectional change for the simple E-B shaft model can be determined by solving the following sets of matrix equations. Only two representative combinations are shown.

Case II ($A_l>0,\ B_l<0$)–*Case II* ($A_r>0,\ B_r<0$):

$$\begin{bmatrix}1 & 1\\ -\mathrm{i}\Gamma_{1l} & -\Gamma_{2l}\end{bmatrix}\mathbf{C}^+ + \begin{bmatrix}1 & 1\\ \mathrm{i}\Gamma_{1l} & \Gamma_{2l}\end{bmatrix}\mathbf{r}\mathbf{C}^+ = \begin{bmatrix}1 & 1\\ -\mathrm{i}\Gamma_{1r} & -\Gamma_{2r}\end{bmatrix}\mathbf{t}\mathbf{C}^+, \tag{B1a}$$

$$\begin{bmatrix}-\Gamma_{1l}^2 & \Gamma_{2l}^2\\ \mathrm{i}\Gamma_{1l}^3 & -\Gamma_{2l}^3\end{bmatrix}\mathbf{C}^+ + \begin{bmatrix}-\Gamma_{1l}^2 & \Gamma_{2l}^2\\ -\mathrm{i}\Gamma_{1l}^3 & \Gamma_{2l}^3\end{bmatrix}\mathbf{r}\mathbf{C}^+ = \begin{bmatrix}-\sigma^4\Gamma_{1r}^2 & \sigma^4\Gamma_{2r}^2\\ \mathrm{i}\sigma^4\Gamma_{1r}^3 & -\sigma^4\Gamma_{2r}^3\end{bmatrix}\mathbf{t}\mathbf{C}^+ \tag{B1b}$$

Case II ($A_l>0,\ B_l<0$)–*Case IV* ($A_r<0,\ B_r<0$):

$$\begin{bmatrix}1 & 1\\ -\mathrm{i}\Gamma_{1l} & -\Gamma_{2l}\end{bmatrix}\mathbf{C}^+ + \begin{bmatrix}1 & 1\\ \mathrm{i}\Gamma_{1l} & \Gamma_{2l}\end{bmatrix}\mathbf{r}\mathbf{C}^+ = \begin{bmatrix}1 & 1\\ -\Gamma_{1r} & -\mathrm{i}\Gamma_{2r}\end{bmatrix}\mathbf{t}\mathbf{C}^+, \tag{B2a}$$

$$\begin{bmatrix} -\Gamma_{1l}^2 & \Gamma_{2l}^2 \\ \mathrm{i}\Gamma_{1l}^3 & -\Gamma_{2l}^3 \end{bmatrix}\mathbf{C}^+ + \begin{bmatrix} -\Gamma_{1l}^2 & \Gamma_{2l}^2 \\ -\mathrm{i}\Gamma_{1l}^3 & \Gamma_{2l}^3 \end{bmatrix}\mathbf{r}\mathbf{C}^+ = \begin{bmatrix} \sigma^4\Gamma_{1r}^2 & -\sigma^4\Gamma_{2r}^2 \\ -\sigma^4\Gamma_{1r}^3 & \mathrm{i}\sigma^4\Gamma_{2r}^3 \end{bmatrix}\mathbf{t}\mathbf{C}^+, \tag{B2b}$$

where Γ_{1r} and Γ_{2r} have been defined in equations (45c, d), and A_r and B_r are given by

$$A_r = -2\beta\tilde{\omega} - 16\,\frac{\varepsilon_r}{\sigma^2}, \qquad B_r = -16\,\frac{\tilde{\omega}^2}{\sigma^2}. \tag{B3a, b}$$

APPENDIX C: REFLECTION MATRICES

The reflection matrices for a group of waves incident upon a general boundary for the E-B shaft model are listed as follows.

Case II ($A > 0,\ B < 0$):

$$\mathbf{r} = \begin{bmatrix} -\Gamma_1(\Gamma_1 - \mathrm{i}\Sigma_m) & \Gamma_2(\Gamma_2 + \Sigma_m) \\ \mathrm{i}\Gamma_1^3 + \Sigma_s & -\Gamma_2^3 + \Sigma_s \end{bmatrix}^{-1} \begin{bmatrix} \Gamma_1(\Gamma_1 + \mathrm{i}\Sigma_m) & -\Gamma_2(\Gamma_2 - \Sigma_m) \\ \mathrm{i}\Gamma_1^3 - \Sigma_s & -\Gamma_2^3 - \Sigma_s \end{bmatrix}; \tag{C1}$$

Case IV ($A < 0,\ B < 0$):

$$\mathbf{r} = \begin{bmatrix} -\Gamma_2(\Gamma_2 - \mathrm{i}\Sigma_m) & \Gamma_1(\Gamma_1 + \Sigma_m) \\ \mathrm{i}\Gamma_2^3 + \Sigma_s & -\Gamma_1^3 + \Sigma_s \end{bmatrix}^{-1} \begin{bmatrix} \Gamma_2(\Gamma_2 + \mathrm{i}\Sigma_m) & -\Gamma_1(\Gamma_1 - \Sigma_m) \\ \mathrm{i}\Gamma_2^3 - \Sigma_s & -\Gamma_1^3 - \Sigma_s \end{bmatrix}, \tag{C2}$$

where

$$\Sigma_m = J_m\,\tilde{\omega}^2 - k_r - \mathrm{i}c_r\,\tilde{\omega} \quad \text{and} \quad \Sigma_s = k_t - m\tilde{\omega}^2 + \mathrm{i}c_t\,\tilde{\omega}. \tag{C3a, b}$$

If the rotating shaft is strain-free, then $\mathbf{r}$ can be reduced to simple forms representing typical boundary conditions such as simple support, clamped support, and free end as shown in reference [6]. Note that for those supports in the strain-free case, the reflection matrices are constant.

APPENDIX D: NOMENCLATURE

A_s	area of shaft cross-section (m^2)
a_0	diameter of shaft cross-section (m)
C	generalized co-ordinate of an incident wave (m)
c_{dt} (c_t)	translational damping coefficient (N·s/m)
c_{dr} (c_r)	rotational damping coefficient (N·m·s/rad)
c_0	bar velocity (m/s)
c_s	shear velocity (m/s)
D	generalized co-ordinate of a transmitted wave (m)
E, G	Young's and shear modulus (N/m^2), respectively
I	lateral moment of inertia of shaft (m^4)
J_M (J_m)	mass moment of inertia of a rotor mass ($kg \cdot m^4$)
K	Timoshenko shear coefficient
K_R (k_r)	rotational spring (N/rad)
K_T (k_t)	translational spring (N/m)
M (m)	mass of rotor (kg)
P	axial force (N)
r_{ij}, t_{ij}	reflection and transmission coefficients, respectively. $i = 1$, positive travelling wave; $i = 2$, negative travelling wave; $j = 1$, propagating wave for *Cases II* and *IV*; $j = 2$, attenuating wave for *Cases II* and *IV*. Both $j = 1, 2$, for propagating wave for *Case I*

$U(u)$	transverse displacement (m)
X-Y-Z (x-y-z)	reference frame co-ordinates (m)

Greeks

α	$(KG)/E$
β	rotation parameter, see equation (1d)
ε	$P/(EA)$, axial strain
ε'	non-dimensional axial load parameter, see equation (13b)
$\bar{\Gamma}$, $\bar{\gamma}$ (Γ, γ)	wavenumber (m^{-1})
$\bar{\eta}$,($\bar{\eta}$)	see equations (20a, b), (22a, b) and (24a, b)
ρ	mass density of shaft (kg/m^3)
σ	diameter ratio between two shaft elements
$\bar{\omega}$, (ω)	frequency of Timoshenko model (rad/s)
$\tilde{\omega}$	frequency of Euler–Bernoulli model (rad/s)
Ω	rotation speed of shaft (rad/s)
$\bar{\psi}$ (ψ)	bending angle of the shaft cross-section (rad)

subscripts l, r	the left and right side of a discontinuity, respectively.
superscript $-$, $+$	negative and positive travelling waves, respectively, when used in C and D; otherwise denotes quantities on the left and right side of a discontinuity respectively.

Note: Symbols in parenthesis are the corresponding non-dimensional parameters.